

$\text{Cu}_2\text{ZnSnSe}_4$
SONOCHEMISTRY SYNTHESIS and CHARACTERIZATION

by
Feifei Feng

A thesis submitted to the Faculty of the University of Delaware in partial fulfillment of the requirements for the degree of Master of Science in Mechanical Engineering

Fall 2013

© 2013 Feifei Feng
All Rights Reserved



SONOCHEMISTRY SYNTHESIS and CHARACTERIZATION

by

Feifei Feng

Approved: _____
S. Ismat Shah, Ph.D.
Professor in charge of thesis on behalf of the Advisory Committee

Approved: _____
Joshua L. Hertz, Ph.D.
Co-Professor in charge of thesis on behalf of the Advisory Committee

Approved: _____
Suresh G. Advani, Ph.D.
Chair of the Department of Mechanical Engineering

Approved: _____
Babatunde A. Ogunnaike, Ph.D.
Dean of the College of Engineering

Approved: _____
James G. Richards, Ph.D.
Vice Provost for Graduate and Professional Education

ACKNOWLEDGMENTS

First, I would like to thank my advisor, Dr Ismat Shah for all the advice and guidance he has provided. Second, I would like to thank all my lab partners for the help they have given to me. I especially want to give my thanks to Dr Emre Yassitepe, Inci Ruzybayev, Roy Murray, Shahzad Hussain and Nopporn Rujisamphan for their help and support on my research. I would also like to say thanks to Alex Delluva for helping me in the experiments. Finally, I would like to thank all my friends and parents who have encouraged and supported me when I was feeling frustrated.

TABLE OF CONTENTS

LIST OF TABLES	vi
LIST OF FIGURES	vii
ABSTRACT	viii

Chapter

1	INTRODUCTION	1
2	EXPERIMENTAL METHODS	4
2.1	Sonochemistry	4
2.2	X-Ray Diffraction	5
2.3	Scanning Electron Microscopy (SEM)	6
2.4	UV-Vis Spectroscopy	6
2.5	Raman Spectroscopy	7
3	SOLID STATE REACTION MODEL	8
3.1	Binary Phase Diagrams	8
3.2	Effective Heat of Formation (EHF) Model	10
3.2.1	Phase Formation Sequence for Cu-Se System	11
3.2.2	Phase Formation Sequence for Sn-Se System	12
3.2.3	Phase Formation Sequence for Zn-Se System	13
3.3	Reaction Path Model (BNDH law)	14
4	SYNTHESIS AND CHARACTERIZATION OF THE QUATERNARY PHASE $\text{Cu}_2\text{ZnSnSe}_4$	17
4.1	Experimental Details	17
4.1.1	Materials	17
4.1.2	Experimental Procedures	17
4.1.3	Characterization	18
4.2	Phase Identification and Characterization	19

4.2.1	Binary systems.....	19
4.2.2	Ternary systems.....	21
4.2.3	Quaternary systems	28
4.2.3.1	XRD and SEM results	28
4.2.3.2	UV-Vis results	32
4.2.3.3	Raman results	33
5	CONCLUSIONS AND RECOMMENDATIONS.....	35
5.1	Summary of Results	35
5.2	Recommendations for Future Work	36
5.2.1	Variation of Sonication and Annealing Parameters	36
5.2.2	Variation of Precursor Mixture Ratios	36
5.2.3	Alternative Solvent and Precursors	37
	REFERENCES.....	38
	Appendix	
	COPYRIGHT PERMISSION DOCUMENTS	42

LIST OF TABLES

Table 3.1:	Crystallographic data of phases involved in the synthesis	15
Table 4.1:	Molecular ratios for different reaction systems.....	18
Table 4.2:	Phase analysis for quaternary samples at different stages.....	30

LIST OF FIGURES

Figure 3.1: Cu-Se phase diagram [15].	8
Figure 3.2: Sn-Se phase diagram [15].	9
Figure 3.3: Zn-Se phase diagram [15].	10
Figure 3.4: EHF plot of Cu-Se system.	12
Figure 3.5: EHF plot of Sn-Se system.	13
Figure 4.1: XRD patterns of as-sonicated a) Zn-Se b) Sn-Se c) Cu-Se samples.	20
Figure 4.2: XRD patterns of 500°C annealed a) Zn-Se b) Sn-Se c) Cu-Se samples.	21
Figure 4.3: XRD patterns of as-sonicated a) Cu-Zn-Se b) Cu-Sn-Se samples.	23
Figure 4.4: XRD patterns of 600°C annealed a) Cu-Zn-Se b) Cu-Sn-Se samples.	24
Figure 4.5: SEM picture of the Cu-Sn-Se 600°C sample.	25
Figure 4.6: SEM micrographs of a) Cu-Se 500°C b) Zn-Se 500°C c) Cu-Zn-Se 500°C.	26
Figure 4.7: X-ray diffraction patterns of the quaternary samples as sonicated and annealed at temperatures from 300°C -600°C. (1)Sn (2) Zn (3) Se (4) CuSe (5) CuSe ₂ (6) cub-Cu ₂ Se (7) ZnSe (8) CZTSe (9) ortho-Cu ₂ Se (10) Cu ₂ SnSe ₄ (11) Cu ₂ SnSe ₃ .	29
Figure 4.8: SEM picture of the CZTSe samples a) as-sonicated; annealed at b) 300°C c) 400°C d) 500°C e) 600°C.	31
Figure 4.9: UV-Vis absorbance spectrum for the CZTSe quaternary 600°C 2hr sample.	32
Figure 4.10: Raman spectrum of CTSe 600°C sample.	33
Figure 4.11: Raman spectrum of CZTSe 600°C 2hr sample.	34

ABSTRACT

With the development of solar cell industry, research on the synthesis of new photovoltaic materials has been developing rapidly. The materials attracting much attention today are the Cu(In,Ga)(S,Se)_2 (CIGSe) materials due to their direct band gap and high absorption coefficient. However, In and Ga in this type of materials are not earth abundant elements. This has made large-scale production of devices based on CIGSe materials very costly. As a substitute, the $\text{Cu}_2\text{ZnSn(S,Se)}_4$ (CZTSe) materials are more environmentally friendly and cheaper compared to CIGSe. CZTSe materials also have direct band gaps and are suitable for solar cell application. These materials have delivered a rather satisfactory performance on devices so far as well. Additionally, Zn and Sn are much cheaper and have more abundant sources.

This research conducts an investigation on the reaction path for the synthesis of the CZTSe particles using sonochemistry. Sonochemistry is a method of using ultrasound irradiation to induce rapid chemical reactions. In this research, the stoichiometrically mixed elemental precursors were first ultrasonicated in the organic solvent 2-cyanopyridine and then dried on the hot plate to be transferred into furnace for annealing in Ar atmosphere. A rapid reaction between Cu and Se was obtained directly after sonication according to x-ray diffraction (XRD) analysis. The effective heat of formation (EHF) model was applied to predict the phase formation sequence. The results obtained from the synthesis matched well with the model.

Moreover, to study the formation paths, a crystallographic model was applied to determine the reaction potential between different phases. First the Bravais-Niggli-

Donna-Harker (BNDH) law was used to predict the most probable facets for the reactant phases. These phases are then compared with each other to check for epitaxial relations by looking for common structures in their most probable crystal planes. Those phases containing structural similarities in at least one of the most probable facets are considered suitable for epitaxy. Epitaxial relations between reactants have been shown to be able to remarkably enhance reaction rates by minimizing the diffusion required for the formation of product lattices. Based on this model, Hergert et al proposed two formation paths for the CZTSe synthesis. The two paths are confirmed by the experiment results in this research. XRD is the major technique used for phase identification. The quaternary CZTSe phase obtained with sonication and post annealing was further confirmed by Raman spectroscopy and UV-Vis results.

Chapter 1

INTRODUCTION

With the exacerbation of global warming and energy problem, the need for newer materials for solar cells has been more acute than ever. These materials, usually semiconductors, form the active layer in the solar cells. They absorb the energy in a particular range of the solar light and generate charge carriers (electron-hole pairs), which are separated to produce current [1].

Therefore, in order to qualify as solar cell materials, the semiconductor materials need to have high absorption for photons within the visible light range. Cu(In,Ga)S_2 (CIGS) and Cu(In,Ga)Se_2 (CIGSe) are widely used absorber materials in solar cells. These materials have a direct band gap tunable between 1.0 eV and 1.7 eV, which matches the range of the visible spectrum in the solar light. They have great performance in solar cell devices with a conversion efficiencies up to 20.3% [2]. However, the downside of this type of material is that In and Ga are not earth abundant elements and thus very costly.

Recently a more environmentally friendly alternative material $\text{Cu}_2\text{ZnSn(S,Se)}_4$ (CZTS,Se) has been the focus of researchers in photovoltaics. CZTSe is an analogue of CIGSe by replacing the Group III In (Ga) element with Group II Zn and Group IV Sn, both of which are nontoxic and abundant elements. They have been proven to be promising candidates for photovoltaic applications. The highest efficiency achieved for solar cells based on this type of materials is reported to be 11.1% [3]. The reported band gap energy range for CZTSe is 0.8-1.6 eV [4], which matches well with the prerequisites for a solar cell absorber materials. Common ways to synthesize CZTSe films include coevaporation [5],

sputtering [6], and pulsed laser deposition [7]. For CZTSe particles, solvothermal method is the common way for the synthesis [8-9]. The solvothermal method usually uses toxic organic compounds as the precursors and the treating process takes a long time.

This research is focused on a simple and cost effective way to synthesize CZTSe particles through solid state reactions of elemental precursors with ultrasound irradiation and post-sonication annealing. The effects of ultrasound sonication on chemical reactions have several aspects. First, acoustic cavitations (formation and destruction of bubbles) create a unique high temperature and pressure environment for reactions to occur. Additionally, the collisions between the reactant particles help improve the reactivity by removing surface oxidants. Furthermore, the free radicals released by the solvent during sonication can act as a catalyst to the reactions [10]. This research explored the formation reaction path and microstructure evolution of binary, ternary selenides and eventually the formation of the quaternary phase.

The thesis consists of five chapters. The first chapter is intended to give a brief introduction to the research and the thesis. Chapter 2 introduces the techniques used in the research. The synthesis of the CZTSe material is carried out with a sonochemistry method. X-ray diffraction and Raman spectroscopy are used for phase characterization. Scanning Electron Microscopy is used for morphological studies. Ultraviolet visible spectroscopy is used for optical analyses. Chapter 3 describes the theoretical models used in this research. The effective heat of formation model is used to predict the formation sequence of binary phases. With the information of the phases formed during annealing, the BNDH law is then applied to determine the reaction paths of the synthesis process.

The experimental procedures and result analyses are described in details in Chapter 4. XRD results for the three binary systems-Cu-Se, Sn-Se, Zn-Se, two ternary systems-Cu-

Sn-Se, Cu-Zn-Se and the quaternary system are closely compared and studied to identify the phases at each stage. The phase formation sequence is well matched with the EHF model. In the Cu-Se system, CuSe is the first phase to form, the next are CuSe₂ and Cu₂Se. In the Sn-Se system, the first phase is SnSe₂, the next phase is SnSe. For the Zn-Se system, ZnSe is the only possible phase. The synthesis reactions were also proven to have followed the reaction paths proposed by Hergert [11] obtained by applying the BNDH law. Raman spectroscopy data further confirmed the existence of the quaternary phase in the sample. Based on the optical measurements obtained with UV-Vis spectroscopy, the band gap of the sample is calculated to be 1.2 eV. This result matches well with the reported values of the band gap of CZTSe compound.

Chapter 5 gives a brief summary of the results obtained from this research as well as recommendations for future work.

Chapter 2

EXPERIMENTAL METHODS

2.1 Sonochemistry

Sonochemistry is the study of the effects of sonic waves in chemical applications. The chemical effects of the sonic waves are not directly associated with the interaction with the chemicals. Ultrasound waves enhance chemical reactions through several means. One of the main aspects, acoustic cavitation, refers to the formation, growth and collapse of bubbles induced by the ultrasound. The kinetic energy of the bubbles convert into thermal energy of the liquid content upon collapse [12]. The resulting local high temperature and pressure as well as the subsequent rapid cooling occur at the bubble interface, creating an extreme condition for chemical reactions. The interface can have temperatures up to ~ 5000 K, pressures of ~ 1000 atm and cooling rates above 10^{10} K/s [10]. Additionally the collision of particles during sonication can help remove surface oxides and create melting at the contact area, thus improving the reactivity of reactants. The acoustic cavitations can also release free radicals from the solvent, which can act as a catalyst for chemical reactions.

Due to its appealing properties, sonochemistry has a wide range of applications. For example, the technology can be used for the modification of polymers and polymer surfaces for various purposes including cleaning and precursor preparation. Moreover, it is widely applied in the process of both the decomposition and synthesis of chemical compounds.

In this study, we used ultrasound irradiation for the synthesis of the photovoltaic compound $\text{Cu}_2\text{ZnSnSe}_4$ from elemental precursors. The research is focused on the

investigation of the formation pathway for the quaternary compound as well as the effects of sonication on the synthesis reactions.

2.2 X-Ray Diffraction

X-ray diffraction is a commonly used method to identify crystal structures and determine crystal parameters. The principles can be intuitively explained by the Bragg's Law. When incoming x-ray beams at an incidence angle of θ strike the atoms of the sample, they are reflected by the parallel crystal planes indexed by the Miller's indices and separated by an interplanar spacing d . When the x-ray waves reflected by two adjacent planes are in phase, which means the difference between the path lengths of the waves is an integral multiple of the wavelength of the x-ray, a constructive diffraction occurs resulting in a reflection of maximum intensity. The relationship can be expressed in the following equation:

$$2d \sin \theta = n\lambda \quad (2.1)$$

where d is the spacing between adjacent crystal planes, n is an integral number representing the order of diffraction, λ is the wavelength of the x-ray [13]. By changing θ , we can get a reflection pattern, in which peak intensities and positions are determined by crystal parameters including unit cell length, d -spacing, etc.

In this research, we used a Rigaku D-Max B powder diffractometer equipped with a monochromator. The sample is mounted on goniometer of the diffractometer and rotated over a 2θ scan range of $10-88^\circ$ at a step size of 0.02° . The x-ray source used in our study is $\text{Cu K}\alpha_{1,2}$ radiation. The characterization is realized by comparing the XRD patterns obtained from the instrument with the Joint Committee on Powder Diffraction Standards (JCPDS) database.

2.3 Scanning Electron Microscopy (SEM)

Scanning electron microscopy (SEM) is used to analyze surface morphology of a specimen. During the imaging process, the sample is scanned with a beam of electrons emitted thermionically from an electron gun. The electrons interact with the atoms on the surface of the sample. The scattered beams, usually the secondary electrons emitted from the atoms excited by the incoming electrons are detected and analyzed by detectors to form an image. SEM can achieve a resolution of less than 1nm.

In this research, we used a field emission scanning electron microscope JEOL JSM-7400F for the imaging. The voltage of the electron source is 10 kv, under which condition the penetration depth into the sample is 1-1.5 μm .

2.4 UV-Vis Spectroscopy

Ultraviolet-visible (UV-Vis) spectroscopy refers to the study of the optical properties of the sample including transmittance, reflectance and absorbance over a wavelength range corresponding to the ultraviolet-visible spectral region. In this research, the experiment was conducted on a Perkin-Elmer UV/Vis/NIR spectrophotometer equipped with an integrating sphere to measure the above properties in order to determine the optical band gap of the sample material. The data were obtained over a range of 300-2500nm. Once we get the measurements, we can calculate the optical absorption coefficient of the sample material using Eq. 2.2 [14] below:

$$\frac{T}{(1-R)^2} = \exp(-\alpha d) \quad (2.2)$$

where T is the percentage transmittance, R is the percentage reflectance, α is the absorption coefficient and d is the thickness of the sample layer. The absorption coefficient is related to the photon energy by Eq 2.3 [14]:

$$(\alpha h\nu)^n = C(h\nu - E_g) \quad (2.3)$$

where $h\nu$ is the photon energy, E_g is the band gap energy, C is a constant and n is equal to 2 for direct band gap and $\frac{1}{2}$ for indirect band gap. In this research, CZTSe sample has a direct band gap. Therefore n equals 2 in our calculation. This equation shows a linear relationship between the value of $(\alpha h\nu)^2$ and the photon energy $h\nu$ in the high absorption region ($\alpha \geq 10^4 \text{ cm}^{-1}$) [14]. Once we calculate the absorption coefficient from Eq. 2.2, the band gap energy can be obtained from the intercept of the straight line fitting the linear section with the energy axis in the $(\alpha h\nu)^2$ vs. $h\nu$ plot.

2.5 Raman Spectroscopy

Raman spectroscopy, is named for the fact that it relies on Raman scattering, or inelastic scattering to work. When a laser beam—usually at the visible range—hits the sample, a photon interacts with the electron cloud and chemical bonds of a molecule and excite it to a virtual energy state. Once the molecule relaxes, it emits a photon of a different energy, thus of a different wavelength from the incoming laser. This process is a light scattering phenomenon. The scattered light is then sent through a monochromator and filtered for only the inelastic Raman scattering part to be analyzed by the detector. The wavelength difference of the scattered light and original light is called a Raman shift and is unique for different molecules. Therefore it can be used in identification applications. The difference is usually measured by wavenumbers which is the number of wavelength per unit distance. The common unit for it is cm^{-1} .

In this research, we used a Senterra R200L dispersive Raman spectrometer with an Olympus microscope module by Bruker Optics to collect the Raman data. The laser lights used in the experiment include a red light with a wavelength of 785 nm at 100 mW and a green light with a wavelength of 532 nm at 20 mW.

Chapter 3

SOLID STATE REACTION MODEL

3.1 Binary Phase Diagrams

Cu-Se system has several phases. At temperatures below 300°C, there are α -CuSe, β -CuSe, Cu_3Se_2 and CuSe_2 , depending on the composition. Important phase transitions occur at 332°C when CuSe_2 transforms to γ -CuSe and Se and at 377°C when γ -CuSe transforms to β - Cu_{2-x}Se and liquid Se.

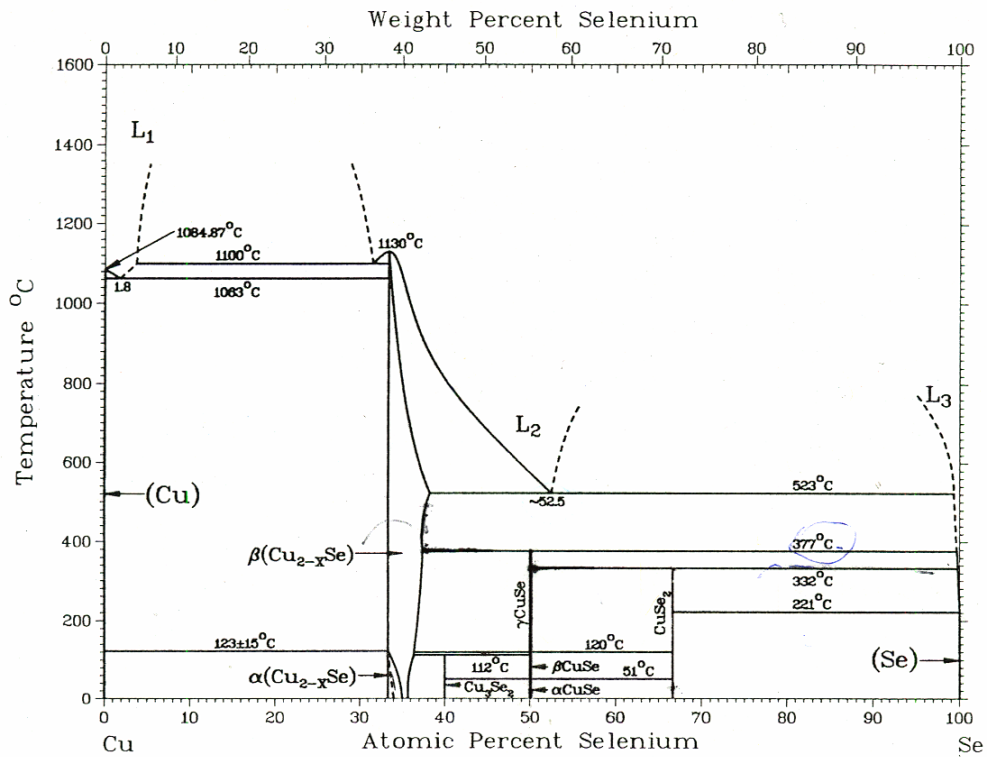


Figure 3.1: Cu-Se phase diagram [15].

The Sn-Se system has only two compound phases, SnSe and SnSe₂. Both of them are stable at high temperatures around 600°C. The eutectic temperature of the system is 628°C.

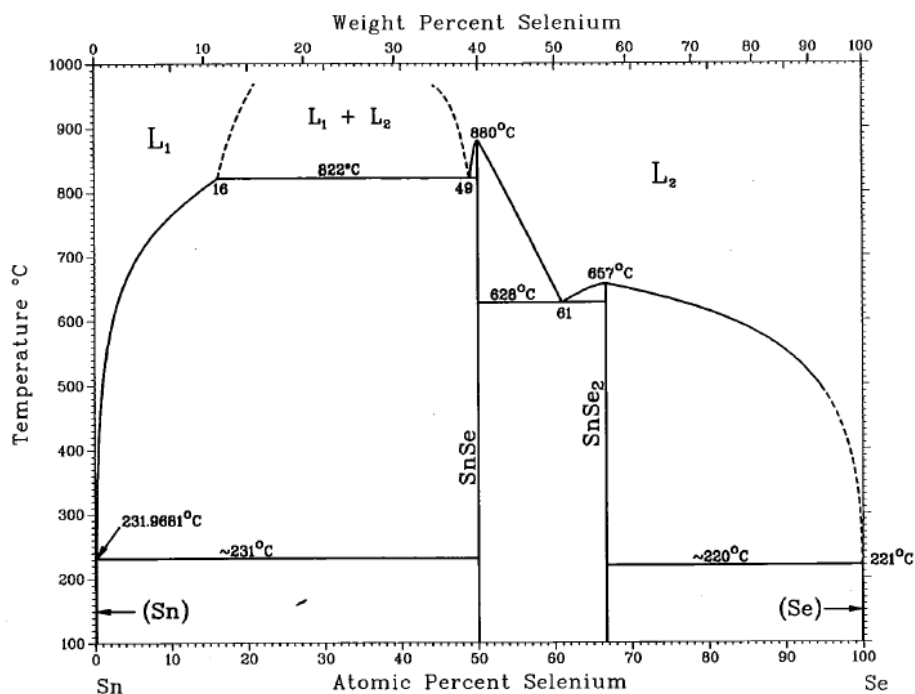


Figure 3.2: Sn-Se phase diagram [15].

The Zn-Se system has only one compound phase ZnSe. It is stable up to about 1300°C. The phase diagram is shown below.

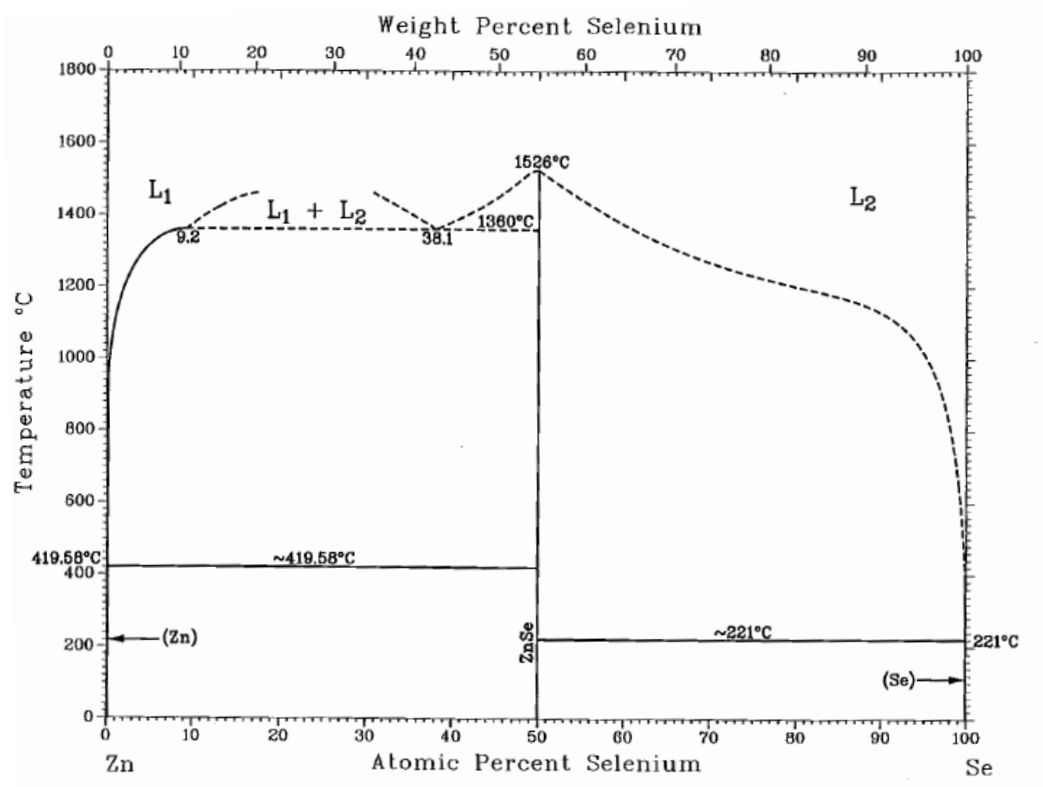


Figure 3.3: Zn-Se phase diagram [15].

3.2 Effective Heat of Formation (EHF) Model

For binary systems, the effective heat of formation (EHF) model was used to predict the formation sequence of binary phases. The driving force for any reaction to take place is the change in Gibbs free energy ΔG .

$$\Delta G = \Delta H_f + T\Delta S \quad (3.1)$$

where ΔH_f is the change of enthalpy, i.e. heat of formation, T is the temperature of the reaction and ΔS is the change of entropy. For solid state reactions, the change in entropy is in the order of 10^{-3} kJ/mol and can be neglected [16]. Therefore, we can use heats of formation

to determine the phase formation sequence for low temperature solid state reactions when there is no activation or nucleation barriers.

In the EHF model, effective heat of formation $\Delta H'$ is used instead of ΔH to take into account the concentration at the growth interface. $\Delta H'$ is defined as:

$$\Delta H' = \Delta H \times \frac{\text{Effective Concentration of Limiting Element}}{\text{Compound Concentration of Limiting Element}} \quad (3.2)$$

where ΔH is the heat of formation of the compound. To use the model to predict phase formation, we need to know the effective concentration at the crystal growth interface for the reaction. It is not possible to calculate the actual concentration at the interface. However, since the highest mobility and therefore the most effective mixing at the interface take place at the lowest eutectic point of the binary system. The effective concentration is assumed to be the composition of the liquidus minimum of the system. The model predicts that the first phase to form is the one with the lowest effective heat of formation at the liquidus minimum. [17-18]

The next phase formed at the interface is decided by the concentration of elements in the mixture. After first phase formation, the sequence moves across the phase diagram to the direction of increasing element which is abundant in the system. [17,19].

3.2.1 Phase Formation Sequence for Cu-Se System

For the Cu-Se system, the heat of formation values for CuSe, CuSe₂ and Cu₂Se are -39.5 kJ/mol, -43.0 kJ/mol and -59.3 kJ/mol, respectively [19]. When used to calculate the effective heat of formation, the above values were transformed to values per atom, which became -19.8 kJ/(mol·atom), -21.5 kJ/(mol·atom) and -29.7 kJ/(mol·atom) respectively. The EHF plot for the Cu-Se system is shown in Fig. 3.4 below. Applying the EHF to the plot, we can see that CuSe is the first phase to be formed since it has the lowest effective heat of

formation value. The next phase to form depends on the element composition at the interface. If Se is abundant, the sequence moves across the phase diagram to the right and the next phase to form is CuSe_2 . If Cu is abundant, the next phase to form is Cu_2Se .

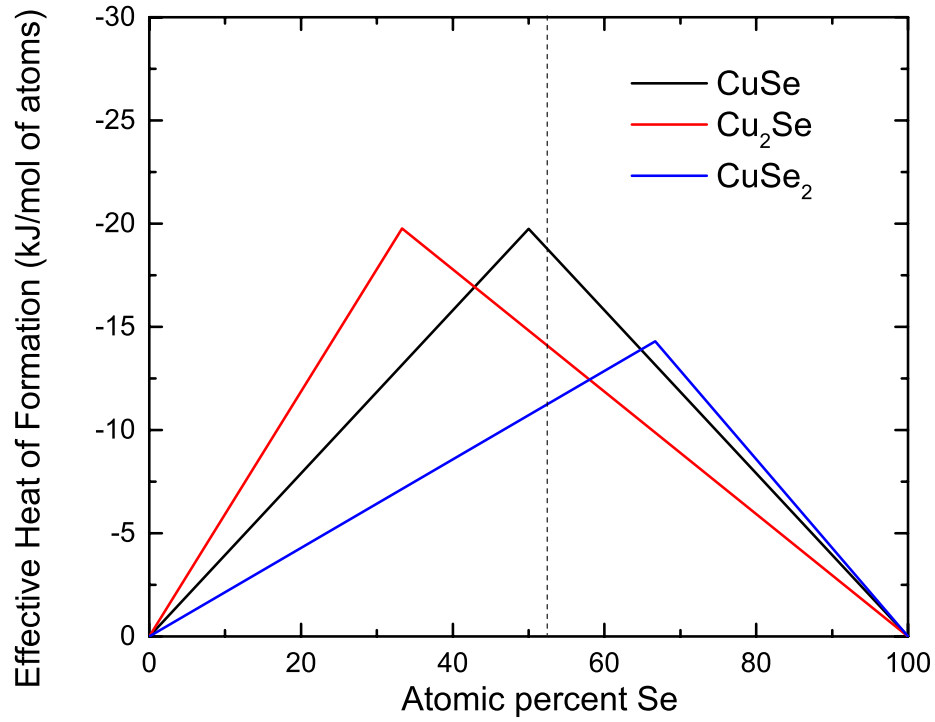


Figure 3.4: EHF plot of Cu-Se system.

3.2.2 Phase Formation Sequence for Sn-Se System

For the Sn-Se system, there are only two reported phases according to the phase diagram, which are SnSe and SnSe_2 . The heat of formation values for the two phases are -68.6 kJ/mol and -124.7 kJ/mol respectively [20]. The values per atom are -34.38

$\text{kJ}/(\text{mol}\cdot\text{atm})$ and $-41.68 \text{ kJ}/(\text{mol}\cdot\text{atm})$ respectively. The EHF plot of the system is shown in Fig. 3.5. According to the plot, SnSe_2 has the lower effective heat of formation, thus will be the first phase to be formed. The next phase to be formed is SnSe .

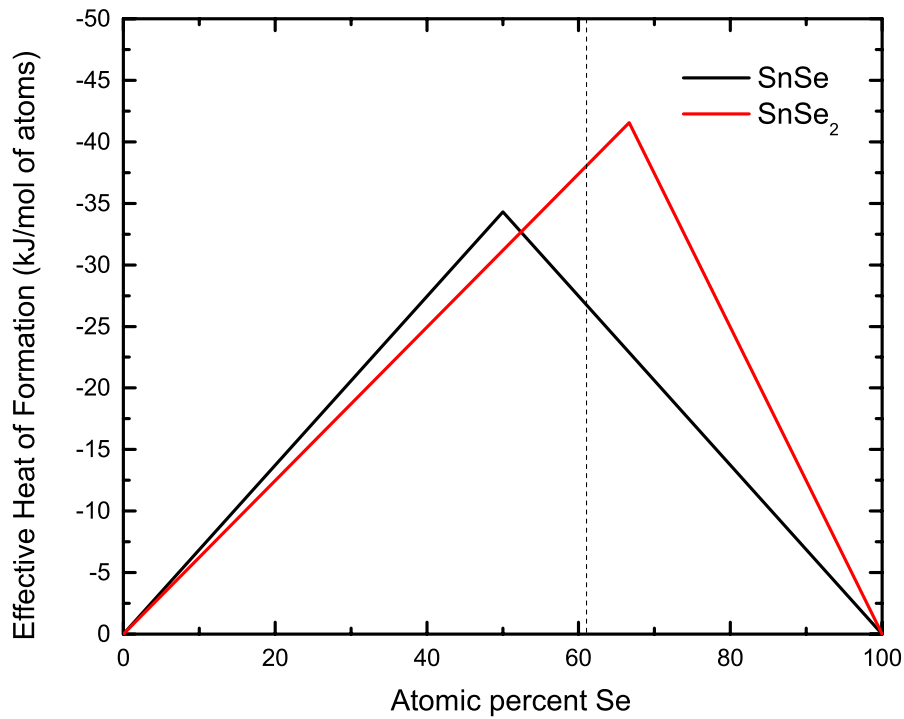


Figure 3.5: EHF plot of Sn-Se system.

3.2.3 Phase Formation Sequence for Zn-Se System

In the Zn-Se system, only one phase exists according to its phase diagram (Fig. 3.3). Therefore, ZnSe will be the only phase to form.

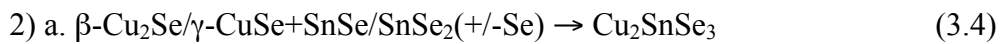
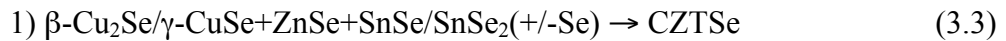
3.3 Reaction Path Model (BNDH law)

To predict the reaction path of the solid state reactions involved in the synthesis, Hergert *et al.* applied the BNDH law to estimate the epitaxial relations between the possible compounds. The BNDH law was named with the initials of the four contributors. It is used to predict the lattice planes faceting the crystal by assuming that the growing speed of a lattice plane is inversely proportional to its reticular density of atoms. The planes with the largest d-spacing will be the most favored facets in the crystal structure and thus primarily serving for the epitaxial growth in the solid state reactions [21]. Based on the BNDH law, they have obtained the first four most probable faces for all the phases involved in the synthesis of CZTSe. The crystallographic data for the phases occurred in the synthesis are presented in Table 3.1 below with the faces listed in the order of the most probable to the least probable. The crystal faces containing the hexagonal unit are indicated in bold [11]. The results were compared to look for epitaxial relations. It has been proposed that the solid state reactions are remarkably enhanced if there exist structural similarities between the reactants [22]. In the synthesis of CZTSe, the common structural unit contained in all the compounds is an anion hexagon of the chalcogen. A phase is considered to be suitable for epitaxy if at least one of the most probably faces contains the hexagon unit. The epitaxy is possible because the anion hexagons in the selenide compounds have very similar averaged anion-anion distances with a maximal difference of 8-9% due to the similar cation radii. According to Shannon [23], the data are as below: $r(\text{Cu}^+)$ is 74 pm, $r(\text{Zn}^{2+})$ is 74 pm, $r(\text{Sn}^{4+})$ is 69 pm, $r(\text{Se}^{2-})$ is 184 pm in tetrahedral coordination. This structure similarity allows a rapid reaction between the reactants by avoiding the rearrangement of chalcogenide sublattice.

Table 3.1: Crystallographic data of phases involved in the synthesis [11]

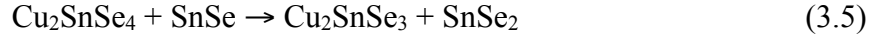
Compound	Space group	Lattice parameters	Expected faces suiting epitaxy
β -Cu ₂ Se	F-43m	a=584.0 pm	{111}
γ -CuSe	P6 ₃ /mmc	a=398.0 pm, c=1725.4 pm	{001}, {100}, {101}, {102}
CuSe ₂	Pnnm	a=500.5 pm, b=618.2 pm, c=374.0 pm [21]	{110}, {011}, {010}, {101}
ZnSe	F-43m	a=561.8 pm	{111}, {100}, {110}, {311}
SnSe	Cmcm	a=430.61 pm, b=1171.1 pm, c=430.61 pm	{010}, {110}, {021}, {111}
SnSe ₂	P-3m1	a=381.08 pm, c=614.10 pm	{001}, {100}, {101}, {102}
Cu ₂ SnSe ₃	Cc	a=696.70 pm, b=1204.93 pm, c=694.53 pm, $\beta=109.19^\circ$	{010}, {110}, {-111}, {021}
Cu ₂ ZnSnSe ₄	I-42m	a=568.82 pm, c=1133.78 pm	{001}, {101}, {110}, {112}

Based on the epitaxial relations, they have proposed two reaction pathways for the synthesis reaction of CZTSe shown in Eq. 3.3 and Eq. 3.4. Eq. 3.3 shows a direct synthesis from the three kinds of binary phases reacting with each other at the same time. β -Cu₂Se, ZnSe and SnSe₂ are the most favorable reactants. These three phases are ionic compounds containing mobile cations and they all provide epitaxy on the first probable crystal face. Also SnSe₂ has a layer structure connected with weak Van-der Waals forces between layers, which makes it easier to shear along the direction perpendicular to the <001> axis. There is a concurring reaction path which is a two-step reaction with the ternary phase Cu₂SnSe₃ as the intermediate product as shown in Eq.3.4 [11].



b. $\text{Cu}_2\text{SnSe}_3 + \text{ZnSe} \rightarrow \text{CZTSe}$

In our experiments, another ternary phase Cu_2SnSe_4 formed when the sample was annealed at 400°C along with Cu_2SnSe_3 . Due to the lack of crystallographic data, we did not obtain the information on Cu_2SnSe_4 forming epitaxial relations with the other phases. According to Yoo *et al.* [3], Cu_2SnSe_4 first formed at about 400°C for compounding the Cu_2SnSe_3 phase following the reaction below:



All the Cu_2SnSe_4 phase transformed to Cu_2SnSe_3 by 500°C , which can form CZTSe following Eq. 3.4b. Therefore, this equation is well matched with the Hergert model.

Chapter 4

SYNTHESIS AND CHARACTERIZATION OF THE QUATERNARY PHASE $\text{Cu}_2\text{ZnSnSe}_4$

4.1 Experimental Details

4.1.1 Materials

Elemental Cu (99%, <75 μm), Zn (99%, -100 mesh), Sn (99.9%, -325 mesh) and Se (99%, -325 mesh) powders purchased from Sigma Aldrich were used as precursors without treatment. Solvent used for ultrasound sonication is 2-cyanopyridine (99%) purchased from ACROS Chemicals.

4.1.2 Experimental Procedures

All the sonication experiments were carried out on a Cole Palmer 500 W, 20 kHz Ultrasonic Homogenizer at a power output of 5-8 W. Metal powders mixed with Se powders in near stoichiometric mole ratios shown in Table 4.1 were made into suspension in a 5ml vial after adding 1ml of 2-cyanopyridine and sonicated for 2 minutes. Cu is kept deficient for Cu-Sn-Se system and the quaternary system to render more complete reactions. Se is kept abundant to compensate for high temperature loss. Nitrogen gas was kept flowing throughout and after the sonication until the suspension cooled down in order to prevent oxidation.

After sonication, the suspension was then transferred to a 1 in² glass substrate on which it was dried on the hot plate for 2 hours at about 60°C. The temperature was kept low to prevent oxidation. Once dried, the samples were placed into the furnace to be annealed at

temperatures between 300 and 600°C in Ar gas atmosphere and cooled down naturally afterwards.

Table 4.1: Molecular ratios for different reaction systems.

Binary system Cu:Se,Sn:Se,Zn:Se	1:2
Ternary system Cu:Zn:Se	1:1:3
Ternary system Cu:Sn:Se	1.8:1:6
Quaternary system Cu:Zn:Sn:Se	1.8:1:1:5 for 500°C and below 1.8:1:1:9 for 600°C 2 hrs

4.1.3 Characterization

Crystal structure and phase identification analyses of the samples were carried out by X-ray diffraction (XRD) on a Rigaku D-max B diffractometer with high-intensity Cu $K\alpha_{1,2}$ radiations. The 2θ scan range used for all the samples was 10 to 88° with a step size of 0.02 degree and a dwelling time of 2 seconds. The morphology is investigated by scanning electron microscopy (SEM) using a JEOL JSM-7400F equipment. UV-Vis data were collected on a Perkin-Elmer UV/Vis/NIR spectrophotometer equipped with an integrating sphere over a wavelength range of 300-2500 nm. Raman data were collected on a Senterra R200L dispersive Raman spectrometer with an Olympus microscope module by Bruker Optics. The laser lights used in the experiment is a red light with a wavelength of 785 nm. The intensity is 25 mW for the ternary sample and 100 mW for the quaternary sample. The resolution for the graph is 9-15 cm^{-1} . The integration time is 9 s for the ternary sample and 100 s for the quaternary sample.

4.2 Phase Identification and Characterization

4.2.1 Binary systems

XRD pattern of the Cu-Se as-sonicated sample (Fig. 4.1c) shows that Cu and Se formed α -CuSe stable at room temperature with excess Se. This result is consistent with the EHF model, which predicts that CuSe is the first phase to form. After annealing at 300°C, the hexagonal high temperature modification γ -CuSe was found in the sample together with the orthorhombic compound CuSe₂ which starts to form at 120°C and is stable up to 332°C. CuSe₂ formed after CuSe because there was abundant Se in the sample, making the sequence moved to the Se-rich direction across the phase diagram. Cu₃Se₂ was skipped because it only exists up to 112 °C [15]. At 400°C, all the CuSe₂ had been transformed into γ -CuSe, part of which then transformed to the face centered cubic β -Cu₂Se stable between 123°C and 1130°C [15] as observed in the sample annealed at 500°C. XRD pattern in Fig. 4.2c clearly shows peaks for cubic Cu₂Se and some CuSe phase.

Sn-Se system showed no reaction in the as-sonicated sample. The XRD pattern of the sample is shown in Fig. 4.1b. It clearly shows only elemental Sn and Se in the sample. The XRD pattern for the 300°C annealed sample shows peaks for SnSe₂ (hexagonal)-the first phase predicted by the EHF model-as well as the SnSe phase (orthorhombic), which is next phase predicted to form. Both of the two phases can exist up to about 628°C, which is the eutectic temperature of the system (Fig.2). However, SnSe and Se are highly volatile at high temperatures (above 400°C), driving the decomposition of SnSe₂ into gaseous SnSe and Se. The Sn loss through desorption of the SnSe phase is also a major driving force for the decomposition of the quaternary phase CZTSe at high temperatures. This issue is further discussed in Section 4.2.3. Due to the desorption of SnSe, SnSe₂ is the dominant phase in the 500°C sample shown in Fig. 4.2b.

Like the Sn-Se system, we did not observe a reaction in the Zn-Se as-sonicated sample. And there is no reaction observed in the Zn-Se sample post-annealed at 500°C as well. This is probably due to the high eutectic temperature of 1360°C for the Zn-Se system. [15]. As shown in the XRD patterns in Fig. 4.1a and Fig. 4.2a, only peaks for elemental Zn and Se are observed in the plot.

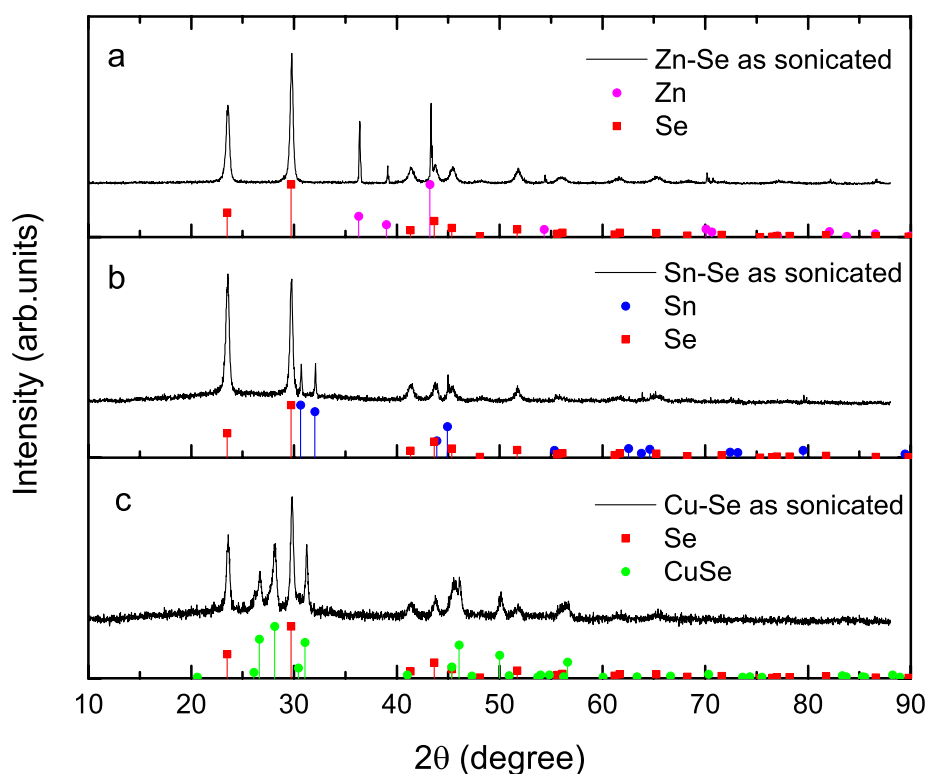


Figure 4.1: XRD patterns of as-sonicated a) Zn-Se b) Sn-Se c) Cu-Se samples.

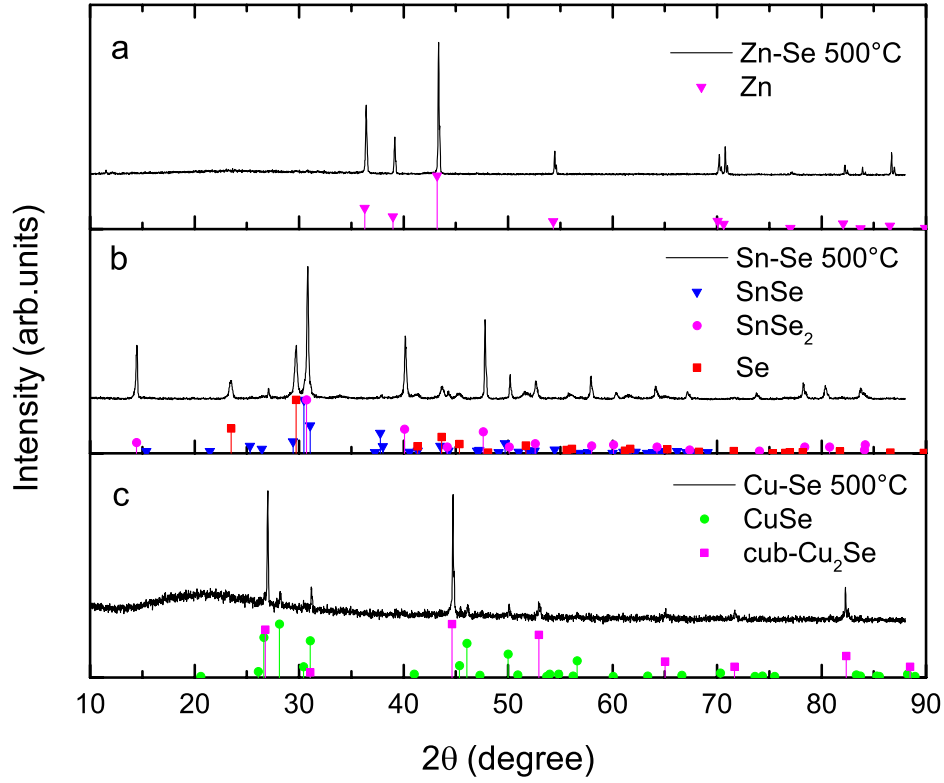


Figure 4.2: XRD patterns of 500°C annealed a) Zn-Se b) Sn-Se c) Cu-Se samples.

4.2.2 Ternary systems

XRD results for the ternary systems are shown in Fig. 4.3 and Fig. 4.4 for as-sonicated samples and 500°C annealed samples, respectively. The pattern for the Cu-Sn-Se (CTSe) as-sonicated sample shows only a reaction between Cu and Se (Fig. 4.3b). After annealed at 300°C, the pattern still shows no sign of reaction between Sn and Se. There are peaks for CuSe and CuSe₂, which is very similar to the Cu-Se binary system 300°C pattern except for peaks corresponding to elemental Sn. We can see that Se reacts with Cu first due to its affinity to chalcogen [3]. For the 400°C annealed sample, XRD pattern shows peaks for the two ternary phases Cu₂SnSe₃ and Cu₂SnSe₄ with a small amount of cubic Cu₂Se. At

500°C, the transformation between the two ternary phases were completed (Eq. 3.5). We achieved a near single phase of Cu_2SnSe_3 with only a minor amount of SnSe and SnSe_2 for samples annealed at 500°C and above. XRD patterns and SEM picture of the 600°C sample are shown in Fig. 4.4b and Fig. 4.5, respectively.

Like the CTSe system, only Cu-Se reaction was observed in the Cu-Zn-Se (CZSe) as-sonicated samples (Fig. 4.3a). In the 300°C annealed sample, XRD pattern shows peaks for CuSe_2 , Zn and some residual Se. There is no reported ternary phase for the Cu-Zn-Se system. Therefore, in the 400°C annealed sample, we found only the binary phases-cubic Cu_2Se , ZnSe and elemental Zn. The 500°C annealed sample however, contained orthorhombic Cu_2Se instead of cubic Cu_2Se . There was also ZnSe and elemental Zn in the sample. In the 600°C sample, ZnSe peak became stronger, indicating a dominant amount of the phase. Both cubic Cu_2Se and orthorhombic Cu_2Se peaks were found in the sample. (Fig. 4.4a)

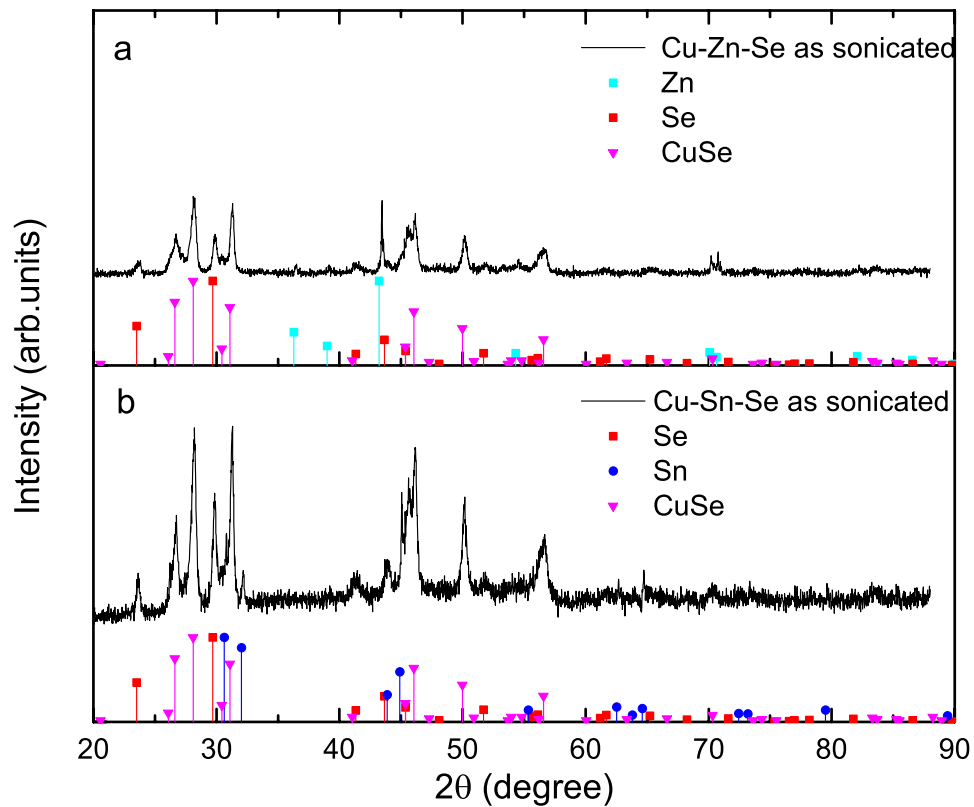


Figure 4.3: XRD patterns of as-sonicated a) Cu-Zn-Se b) Cu-Sn-Se samples.

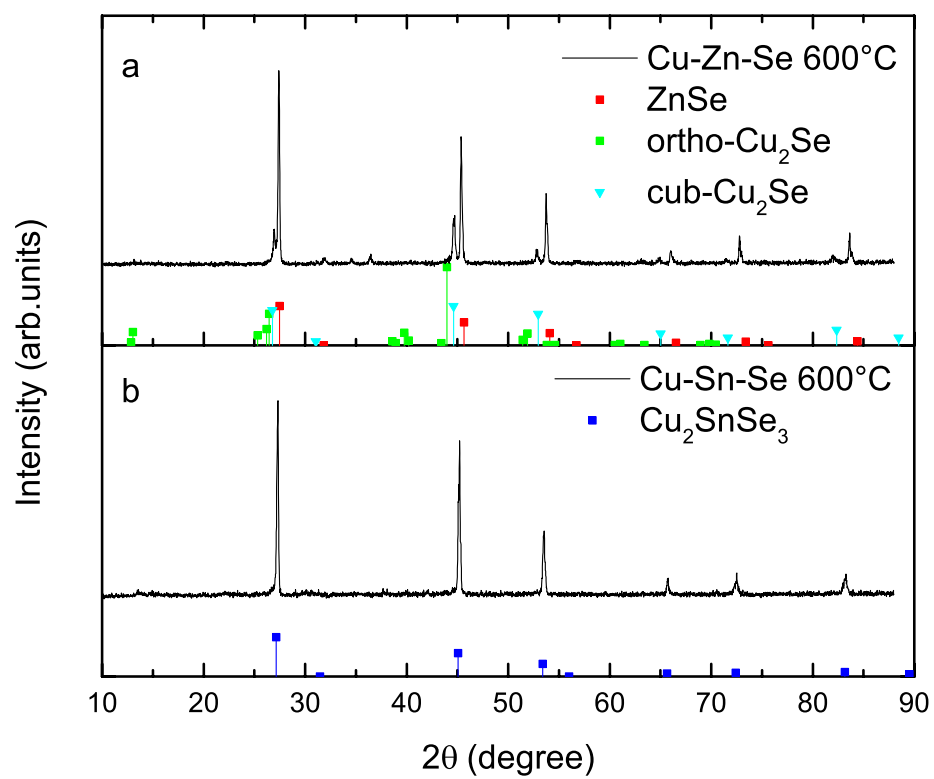


Figure 4.4: XRD patterns of 600°C annealed a) Cu-Zn-Se b) Cu-Sn-Se samples.

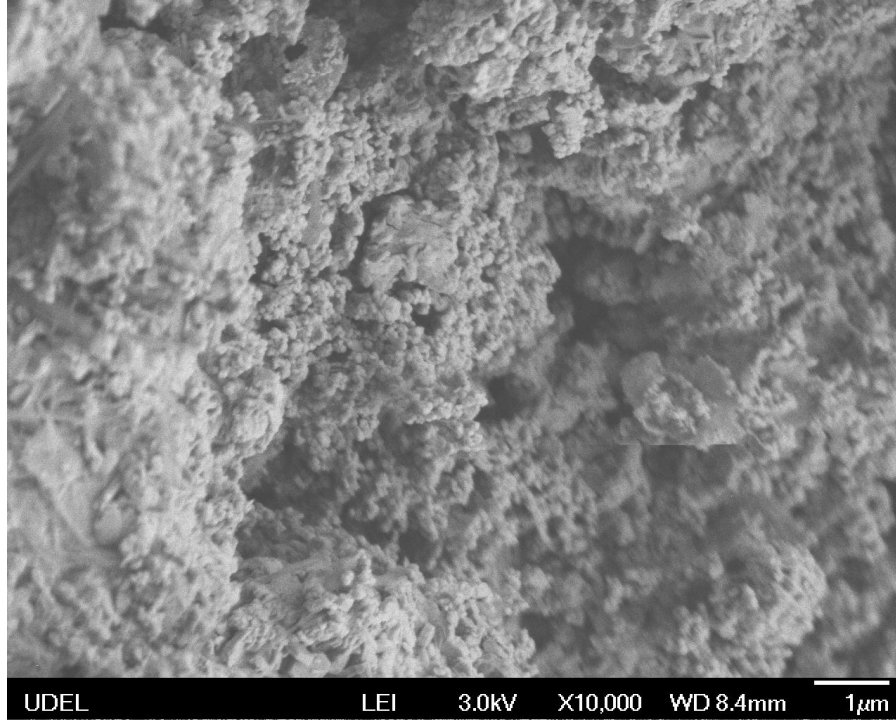


Figure 4.5: SEM picture of the Cu-Sn-Se 600°C sample.

Considering that we did not see any reaction between Zn and Se, we suggest that the formation of ZnSe phase in the CZSe system is attributed to the existence of Cu. We suppose that Cu catalyzed the selenization reaction of Zn. This result can be explained by the metal reactivity theory. Zn is above Cu in the activity series of metal because it has lower electronegativity. At temperatures above 400°C, Cu has already been selenized and exists mainly in the form of Cu^+ in Cu_2Se . Due to the lower electronegativity, it is easier for Zn to lose electrons to Se. Therefore, it can reduce the Cu^+ ion in Cu_2Se and then bond with Se instead following the reaction:



The enthalpy change of the reaction is -109 kJ/mol [24]. The negative value suggests that the reaction is exothermic and spontaneous going in the right direction. After being reduced, Cu

continues to react with Se to form more Cu_2Se . The reaction completed in the 600°C sample where all Zn was reacted and transformed to ZnSe . The SEM micrographs of the Cu-Se 500°C , Zn-Se 500°C and Cu-Zn-Se 500°C samples are shown in Fig. 4.6. Fig. 4.6a displays the agglomerated cubic Cu_2Se crystals. Fig. 4.6b displays the large Zn particle chunks of diameters of $\sim 6\mu\text{m}$. In the ternary picture, we can see the hexagonal Zn particles in the center. The background contains mainly agglomerated cubic ZnSe and some fused orthorhombic Cu_2Se crystals in the lower left corner.

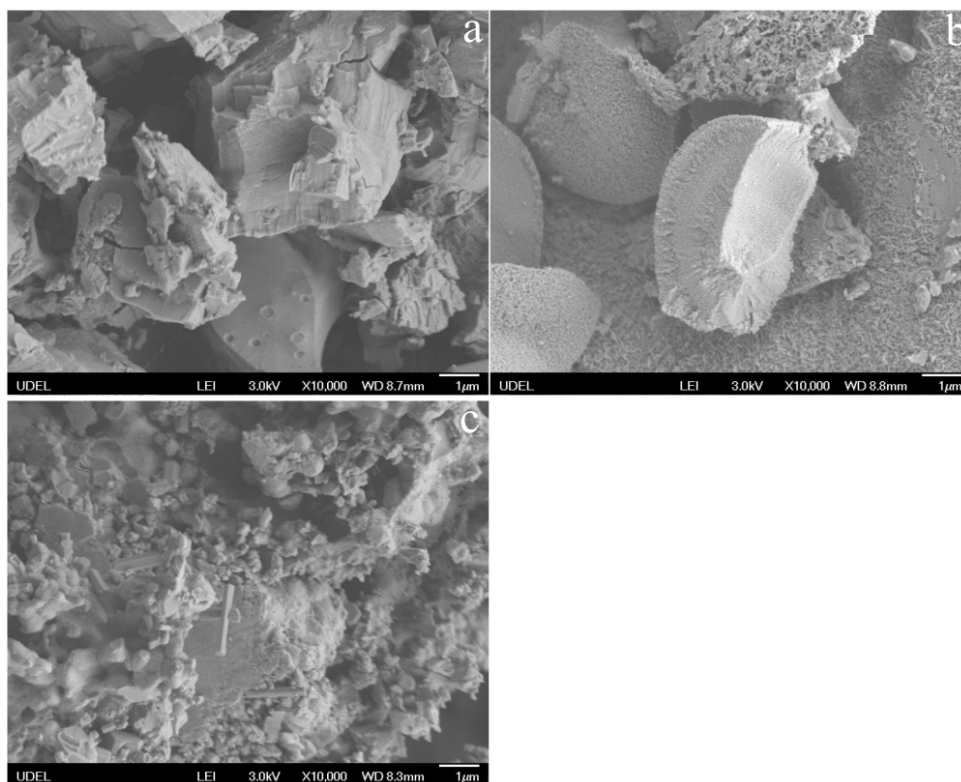


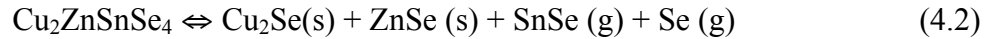
Figure 4.6: SEM micrographs of a) Cu-Se 500°C b) Zn-Se 500°C c) Cu-Zn-Se 500°C .

Another phenomenon that needs to be pointed out is the existence of two phases of Cu₂Se - cubic Cu₂Se and orthorhombic Cu₂Se. Stevels *et al.* [25] have reported the phase transformation from the f.c.c lattice of Cu_{2-x}Se (obtained by reaction of Cu and Se under high temperature) to a less symmetric orthorhombic phase during the cooling process. The temperature for the transformation depends on the value of x, i.e. the Cu vacancies. They observed that it occurred at 140°C for x=0 and at -20°C at x=0.2. In fact, it has been long known that Cu₂Se undergoes a phase transformation during cooling. But the results for the studies of the room temperature phase structure are still controversial. First in 1945, Borchert [26] reported a tetragonal cell. Later in 1971, Stevels *et al.* proposed an orthorhombic structure as mentioned above. Then in 1976, Murray and Heyding [27] proposed a monoclinic structure. Also in 1981, Vucic *et al.* [28] proposed a different monoclinic structure. In 1988, Kashida *et al.* [29] reported a phase transformation for Cu₂Se from a cubic structure to a room temperature pseudo-monoclinic structure, similar to the one proposed by the Vucik group. In our research, we believe the phase we obtained has an orthorhombic structure by comparing the XRD pattern and the JCPDS database. During annealing, the sample was left to cool down naturally in the furnace after heating is turned off. Usually we waited for the samples to cool down to room temperature before taking out for characterization. The orthorhombic Cu₂Se phase is observed in these samples since the transformation had started before the temperature reached room temperature. But there are some cases where the samples were taken out from the furnace before cooling down to room temperature. In these cases, only the cubic phase is observed. Phase transformation will not occur if the sample is quenched down to room temperature instead of letting it cool down slowly. Also, the transformation tends to occur for samples annealed at higher temperature, probably due to the longer cooling time.

4.2.3 Quaternary systems

4.2.3.1 XRD and SEM results

XRD patterns of quaternary samples as-sonicated and annealed at different temperatures are shown in Fig. 4.7. The as-sonicated sample shows only peaks for CuSe as well as elemental phases of Sn, Se and Zn, like the other systems. After annealing at 300°C, we can see peaks for elemental Zn and Sn phases as well as CuSe and CuSe₂ just as the CTSe sample annealed at the same temperature except for the elemental Zn. We started to see the quaternary phase CZTSe peaks in the XRD pattern in the 400°C annealed sample. Ternary phase Cu₂SnSe₃ and Cu₂SnSe₄ are first observed at 400°C, as in the ternary samples. The quaternary phase was quickly formed from the reaction between Cu₂SnSe₃ and ZnSe with an epitaxial relation (Eq. 3.4b). However, the reaction was not completed due to the incomplete synthesis of ZnSe. As a result, abundant Zn and Cu₂SnSe₃ were left in the sample. Once the quaternary phase is formed, it can decompose according to the following equilibrium proposed by Redinger *et al.* [30]:



The decomposition rate varies with different experiment conditions. In our experiment, Ar gas is flowing throughout the annealing and cooling process to prevent oxidation. The Ar gas may have slowed down the desorption of the SnSe phase, thus the decomposition rate of CZTSe [31]. At 500°C, the transition from the ternary phase Cu₂SnSe₄ to Cu₂SnSe₃ is completed following the reaction in Eq. 3.5. Only Cu₂SnSe₃ phase was observed in the sample. After annealing at 600°C for 2 hours, the reactions in Eq. 3.3 and Eq. 3.4 were all completed. All the CTSe ternary phase transformed to the quaternary phase. Small amounts of orthorhombic Cu₂Se phase persists in both 500°C and 600°C samples. Quaternary phase peaks show a tendency to become stronger as the annealing temperature becomes higher. At

700°C, we observed only ortho-Cu₂Se, Cu₂SnSe₃ and ZnSe phases in the sample. The decomposition of the quaternary phase becomes significant at such a high temperature due to drastic loss of SnSe and Se.

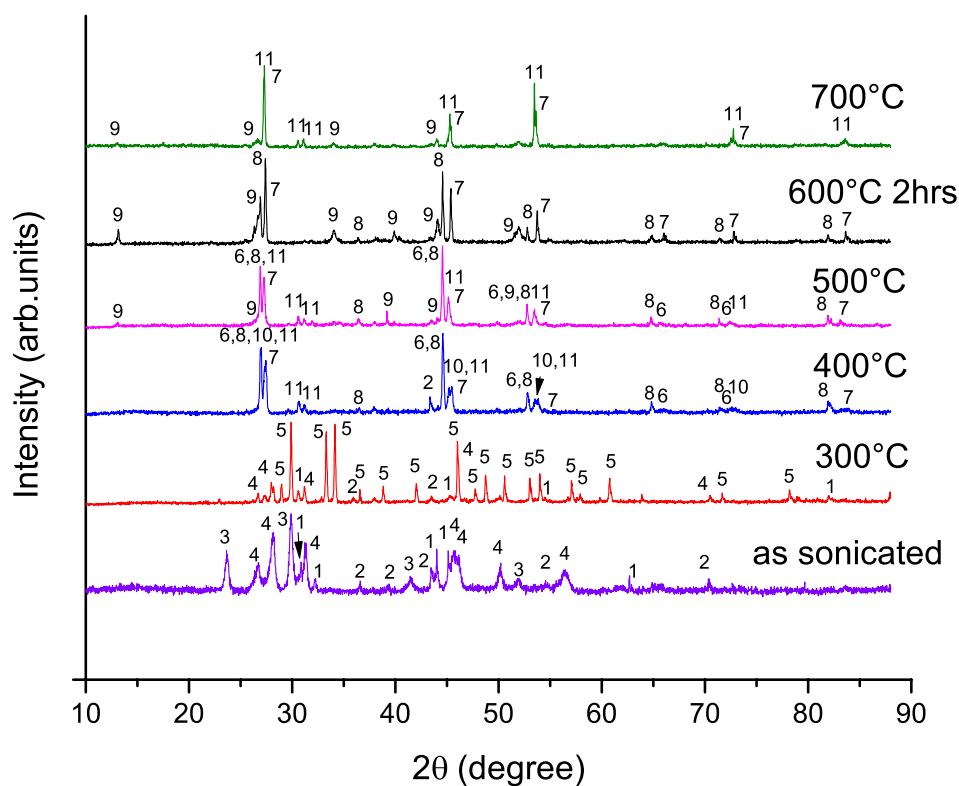


Figure 4.7: X-ray diffraction patterns of the quaternary samples as sonicated and annealed at temperatures from 300°C -600°C. (1)Sn (2) Zn (3) Se (4) CuSe (5) CuSe₂ (6) cub-Cu₂Se (7) ZnSe (8) CZTSe (9) ortho-Cu₂Se (10) Cu₂SnSe₄ (11) Cu₂SnSe₃.

The phase analysis results for the quaternary samples at different stages obtained from the XRD patterns are summarized in Table 4.2 below

Table 4.2: Phase analysis for quaternary samples at different stages.

As sonicated	CuSe, Sn, Se, Zn
300°C	Zn, Sn, CuSe, CuSe ₂
400°C	Zn, cub-Cu ₂ Se, CZTSe, Cu ₂ SnSe ₃ , Cu ₂ SnSe ₄ ,
500°C	ortho-Cu ₂ Se, cub- Cu ₂ Se, CZTSe, Cu ₂ SnSe ₃ ,
600°C 2hrs	ortho-Cu ₂ Se, CZTSe, ZnSe
700°C	ortho-Cu ₂ Se, ZnSe, Cu ₂ SnSe ₃

The morphological evolution of the sonication and annealing process is studied with SEM. Fig. 4.8 shows the SEM micrographs of the quaternary samples as sonicated and annealed at different temperatures. The as-sonicated sample displays a hexagonal CuSe phase showing the {001} facets, the most probable facets for CuSe as predicted by the BNDH law described in Chap. 3. The 300°C sample shows mainly the sintered grains of the orthorhombic CuSe₂ phase. CZTSe phase starts to form between 300°C and 400°C. Fig. 4.8c and Fig. 4.8d display the agglomerated quaternary nanoparticles with some large crystal grains. The crystals shown in Fig. 4.8c are probably the ternary phases. In Fig. 4.8d we can see the triangular shaped Cu₂Se crystal grains showing the {111} facets. Lastly in Fig. 4.8e for the sample annealed at 600°C for 2 hours, we can see the quaternary particles become more prominent.

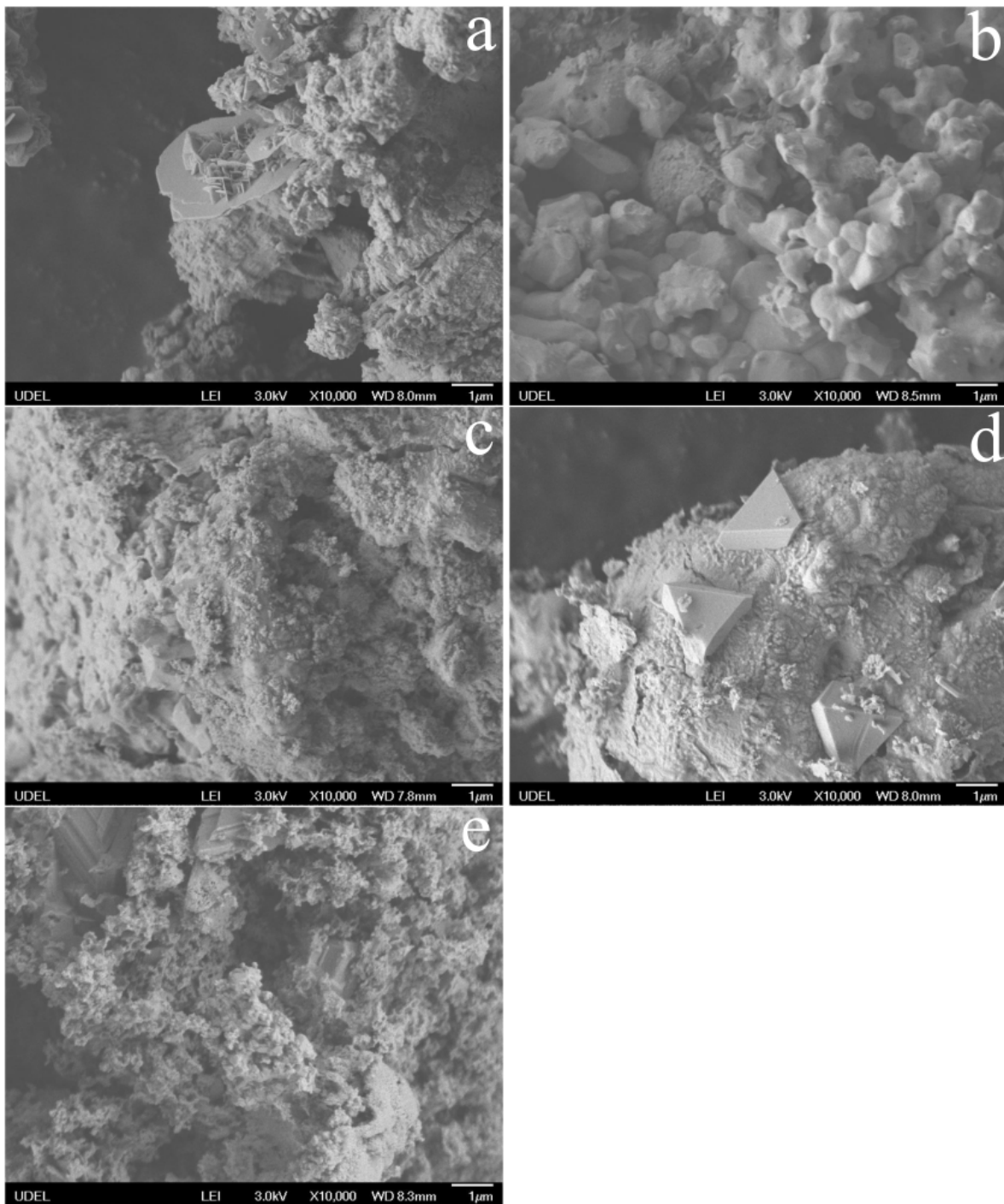


Figure 4.8: SEM picture of the CZTSe samples a) as-sonicated; annealed at b) 300°C c) 400°C d) 500°C e) 600°C.

4.2.3.2 UV-Vis results

The optical properties were measured for the 600°C 2h annealed quaternary sample over a wavelength range of 300-2500 nm. The results are plotted in Fig. 4.9 showing the absorbance curve vs. wavelength in the visible range with an inset plot of $(\alpha h\nu)^2$ as a function of photon energy. The discontinuity in the absorbance curve is due to the change of lamp in the device at the wavelength of 850 nm. The band gap energy obtained from $(\alpha h\nu)^2$ as a function of photon energy plot is 1.2 eV, which is in good agreement with the reported values in the literature indicating the existence of the quaternary compound [8,30,31].

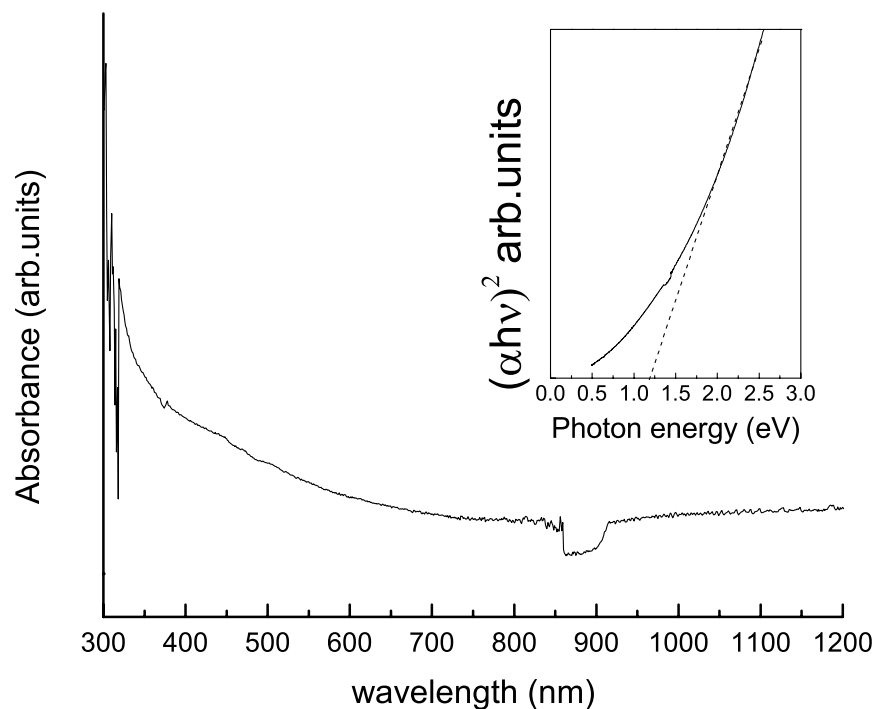


Figure 4.9: UV-Vis absorbance spectrum for the CZTSe quaternary 600°C 2hr sample.

4.2.3.3 Raman results

Raman spectroscopy was performed on both the CTSe ternary and quaternary samples annealed at 600°C. Fig. 4.10 below shows the Raman spectrum of the CTSe 600°C sample. The plot shows a strong sharp peak at 180 cm^{-1} , a lower energy peak at 232 cm^{-1} and a very small peak at 259 cm^{-1} . All three peaks match well with the reported Raman peak positions for Cu_2SnSe_3 phase [33].

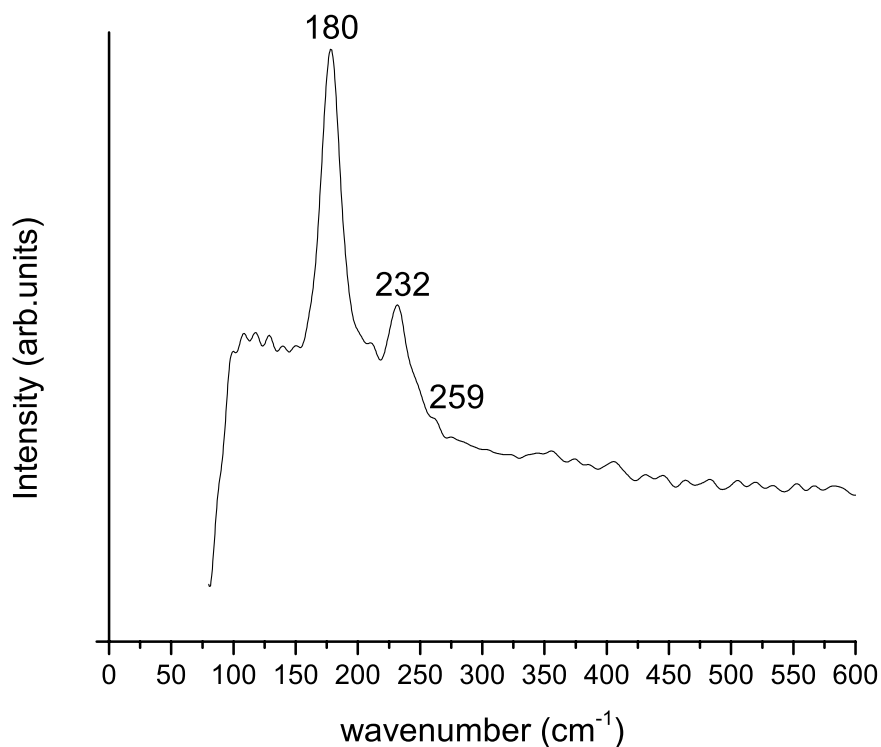


Figure 4.10: Raman spectrum of CTSe 600°C sample.

The Raman spectrum for the quaternary sample annealed at 600°C for two hours is shown in Fig. 4.11. The sharp peak at 248 cm^{-1} is due to ZnSe phase [33]. Raman peaks of

CZTSe were reported [4] to occur at 175 cm^{-1} , 196 cm^{-1} , 234 cm^{-1} and 390 cm^{-1} . The peak at 190 cm^{-1} and 391 cm^{-1} in Fig. 4.11 are clearly due to CZTSe phase. The 175 cm^{-1} and 234 cm^{-1} peaks are not visible probably due to low resolution. The peak at 139 cm^{-1} is due to SnSe [34]. SnSe phase does not appear in XRD pattern probably due to difference in sensitivity of the two techniques. The Senterra Raman spectrometer has a sensitivity of 0.2% while the sensitivity for the Rigaku XRD equipment is about 1%. The peak at 280 cm^{-1} is due to Cu_2Se [35].

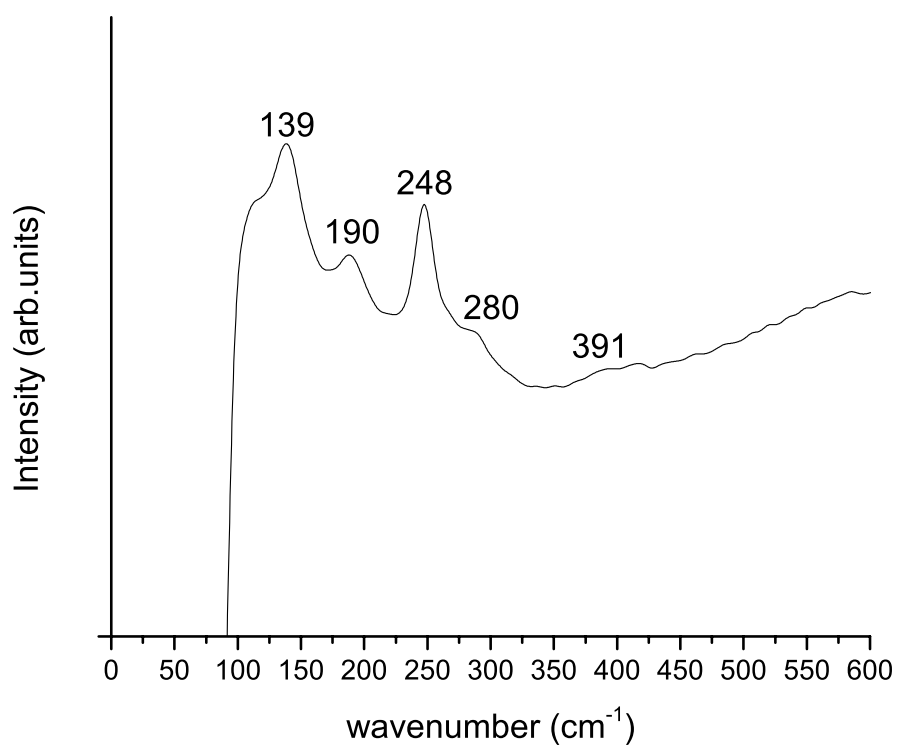


Figure 4.11: Raman spectrum of CZTSe 600°C 2hr sample.

Chapter 5

CONCLUSIONS AND RECOMMENDATIONS

5.1 Summary of Results

In this research, a sonochemistry method has been used to study the formation paths of the photovoltaic material $\text{Cu}_2\text{ZnSeSe}_4$. Sonochemistry is a technique that uses ultrasound irradiation to promote reactions and enhance reaction rates. XRD technique has been used for major phase identification. SEM technique has been used for morphological studies. Other techniques including Raman spectroscopy and UV-Vis spectroscopy were also used for further confirming the formation of the target material.

The synthesis was carried out first by sonicating the elemental precursors with ultrasound in organic solvent and then annealing the dried samples in the furnace. 2-cyanopyridine is used as the solvent in all the sonication experiments. XRD results show that only a reaction between Cu and Se elemental precursors was observed after direct sonication. Post sonication annealing is required for further reactions. The EHF predicts the first phase to form for the binary systems are CuSe, SnSe₂ and ZnSe respectively. SnSe and SnSe₂ phases formed before 300°C during annealing with SnSe₂ being the first phase to form and SnSe next as predicted. There was no reaction observed between Zn and Se in the binary systems. The CTSe ternary system formed two ternary phases Cu_2SnSe_4 and Cu_2SnSe_3 at 400°C. All the Cu_2SnSe_4 phase transformed to the Se-poor phase Cu_2SnSe_3 by 500°C. Raman data showed that we obtained a single phase Cu_2SnSe_3 at 600°C. For the CZSe system, the ZnSe was observed in the samples starting from 400°C. We believe that the existence of Cu catalyzed the reaction between Zn and Se. For the quaternary system, CZTSe started to form in samples annealed at 400°C and above. The quaternary phase starts

to decompose as soon as it forms and keeps a chemical equilibrium. The XRD peaks for the quaternary phase become stronger as the temperature gets higher. Two phases of Cu_2Se were found in the samples, the cubic $\beta\text{-Cu}_2\text{Se}$ and the orthorhombic Cu_2Se . We believe that Cu_2Se undergoes a phase transformation during the natural cooling process. We did not obtain a single phase CZTSe. ZnSe and Cu_2Se were also found in the 600°C 2h annealed sample. At 700°C , the decomposition reaction becomes so significant that only Cu_2Se , Cu_2SnSe_3 and ZnSe exist in the sample. The band gap energy of the sample measured from the UV-Vis data is 1.2 eV, which matches with the reported values for the CZTSe materials.

5.2 Recommendations for Future Work

5.2.1 Variation of Sonication and Annealing Parameters

In this research, all the sonication experiments are conducted under the same conditions. The sonication power is 5-8 W and duration time is 2 minutes. We only obtained a reaction for Cu and Se after direct sonication. Further experiments can be conducted for longer sonication time and with pulsations to achieve a more thorough mixture of the precursors. With different conditions of sonication, it will be interesting to see if we can achieve reactions for Sn-Se or Zn-Se with direct sonication.

We have found that Cu_2Se undergoes a phase transformation during the cooling process. In this research, we did not control the cooling rate of the sample. If there was a systematic control of the cooling rate, we could in turn have a better control of the phase transformation.

5.2.2 Variation of Precursor Mixture Ratios

All the ternary and quaternary samples are mixed nearly stoichiometrically with deficient Cu to achieve more complete reactions and abundant Se to compensate for Se loss

during annealing. Since Sn loss is a major driving force for the quaternary phase decomposition at high temperature, it is advisable to incorporate abundant Sn in the form of SnSe in the mixture precursors. The Zn/Sn ratio in the precursor mixture can be adjusted to obtain the best results.

5.2.3 Alternative Solvent and Precursors

2-cyanopyridine is the only solvent used in the sonication experiments because it does not react with the precursors and is stable at room temperature. Other organic solvent can be investigated as a replacement for better solubility of the elemental precursors and better irradiation effects. Common solvents used in the synthesis include oleylamine (OLA) [36], hexadecylamine (HDA) [2] and mixture of oleic acid and hexadecane [37].

Also, the use of organic precursors in place of elemental metals in sonication is also worth investigation. Wang et al obtained different phases of the quaternary CZTSe nanocrystals using different Se sources including diphenyl diselenide, selenourea and Se powder [37].

REFERENCES

- [1] A. Luque and S. Hegedus, *Handbook of Photovoltaic Science and Engineering*. Chichester: John Wiley & Sons, 2003.
- [2] M. Ahmadi, S. S. Pramana, S. K. Batabyal, C. Boothroyd, S. G. Mhaisalkar, and Y. M. Lam, "Synthesis of Cu_2SnSe_3 nanocrystals for solution processable photovoltaic cells.," *Inorganic chemistry*, vol. 52, no. 4, pp. 1722–8, Feb. 2013.
- [3] H. Yoo, R. A. Wibowo, A. Hölzing, R. Lechner, J. Palm, S. Jost, M. Gowtham, F. Sorin, B. Louis, and R. Hock, "Investigation of the solid state reactions by time-resolved X-ray diffraction while crystallizing kesterite $\text{Cu}_2\text{ZnSnSe}_4$ thin films," *Thin Solid Films*, vol. 535, pp. 73–77, May 2013.
- [4] Y.-F. Du, J.-Q. Fan, W.-H. Zhou, Z.-J. Zhou, J. Jiao, and S.-X. Wu, "One-step synthesis of stoichiometric $\text{Cu}_2\text{ZnSnSe}_4$ as counter electrode for dye-sensitized solar cells.," *ACS applied materials & interfaces*, vol. 4, no. 3, pp. 1796–802, Mar. 2012.
- [5] G. Suresh Babu, Y. B. Kishore Kumar, P. Uday Bhaskar, and V. Sundara Raja, "Growth and characterization of co-evaporated $\text{Cu}_2\text{ZnSnSe}_4$ thin films for photovoltaic applications," *Journal of Physics D: Applied Physics*, vol. 41, no. 20, p. 205305, Oct. 2008.
- [6] R. A. Wibowo, W. S. Kim, E. S. Lee, B. Munir, and K. H. Kim, "Single step preparation of quaternary thin films by RF magnetron sputtering from binary chalcogenide targets," *Journal of Physics and Chemistry of Solids*, vol. 68, no. 10, pp. 1908–1913, Oct. 2007.
- [7] R. Adhi Wibowo, E. Soo Lee, B. Munir, and K. Ho Kim, "Pulsed laser deposition of quaternary $\text{Cu}_2\text{ZnSnSe}_4$ thin films," *Physica Status Solidi (a)*, vol. 204, no. 10, pp. 3373–3379, Oct. 2007.
- [8] A. Shavel, J. Arbiol, and A. Cabot, "Synthesis of quaternary chalcogenide nanocrystals: Stannite," *Journal of the American Chemical Society*, vol. 132, no. 13, pp. 4514–4515, 2010.

- [9] Y.-F. Du, W.-H. Zhou, Y.-L. Zhou, P.-W. Li, J.-Q. Fan, J.-J. He, and S.-X. Wu, "Solvothermal synthesis and characterization of quaternary $\text{Cu}_2\text{ZnSnSe}_4$ particles," *Materials Science in Semiconductor Processing*, vol. 15, no. 2, pp. 214–217, Apr. 2012.
- [10] K. S. Suslick and G. J. Price, "Application of ultrasound to materials chemistry," *Annu. Rev. Mater. Sci.*, vol. 29, pp. 295–326, 1999.
- [11] F. Hergert and R. Hock, "Predicted formation reactions for the solid-state syntheses of the semiconductor materials Cu_2SnX_3 and $\text{Cu}_2\text{ZnSnX}_4$ ($X = \text{S}, \text{Se}$) starting from binary chalcogenides," *Thin Solid Films*, vol. 515, no. 15, pp. 5953–5956, May 2007.
- [12] C. Einhorn, J. Einhorn, and J.-L. Luche, "Sonochemistry-the use of ultrasound waves in synthetic organic chemistry," *Synthesis*, no. 11, pp. 787–813, 1989.
- [13] B. E. Warren, *X-ray Diffraction*. Courier Dover Publications, 1969.
- [14] M. Dongol, "Optical absorption and structural properties of as-deposited and thermally annealed As-Te-Ga thin films," no. 25, pp. 33–47, 2002.
- [15] T. B. Massalski, *Binary Alloy Phase Diagrams*, Second Edi. ASM International, 1990.
- [16] H. J. Moore, D. L. Olson, and R. Noufi, "Use of the effective heat of formation model to determine phase formation sequences of In-Se, Ga-Se, Cu-Se and Ga-In multilayer thin films," *Journal of Electronic Materials*, vol. 27, no. 12, pp. 1334–1340, 1998.
- [17] R. Pretorius, A. M. Vredenberg, F. W. Saris, and R. de Reus, "Prediction of phase formation sequence and phase stability in binary metal-aluminum thin-film systems using the effective heat of formation rule," *Journal of Applied Physics*, vol. 70, no. 7, p. 3636, 1991.
- [18] R. Pretorius, T. K. Marias, and C. C. Theron, "Thin film compound phase formation sequence: An effective heat of formation model," *Materials Science and Engineering*, vol. 10, pp. 1–83, 1993.
- [19] D. Cahen, "Free energies and enthalpies of possible gas phase and surface reactions for preparation of CuInSe_2 ," *J. Phys. Chem. Solids*, vol. 53, no. 8, pp. 991–1005, 1992.
- [20] S. Boone and O. J. Kleppa, "Enthalpies of formation for Group IV selenides (GeSe_2 , $\text{GeSe}_2(\text{am})$, SnSe , SnSe_2 , PbSe) by direct-combination drop calorimetry," *Thermochimica Acta*, vol. 197, pp. 109–121, 1992.

- [21] F. Hergert, S. Jost, R. Hock, and M. Purwins, "A crystallographic description of experimentally identified formation reactions of $\text{Cu}(\text{In,Ga})\text{Se}_2$," *Journal of Solid State Chemistry*, vol. 179, no. 8, pp. 2394–2415, Aug. 2006.
- [22] A. R. West, *Solid State Chemistry and Its Applications*. John Wiley & Sons, 1984.
- [23] R. D. Shannon, "Revised effective ionic radii and systematic studies of interatomic distances in halides and chalcogenides," *Acta Cryst.*, vol. A.32, no. 751, 1976.
- [24] R. C. Weast, *CRC Handbook of Chemistry and Physics*, 58th ed. CRC Press, 1977.
- [25] A. Stevels and F. Jellinek, "Phase transitions in copper chalcogenides: I. The copper-selenium system," *Recueil des Travaux Chimiques des Pays-Bas*, vol. 90, no. 3, pp. 273–283, 1971.
- [26] W. Borchert, "Gitterumwandlungen im System Cu_{2-x}Se ," *Z. Kristallogr.*, vol. 106, pp. 5–24, 1945.
- [27] R. D. Heyding and R. M. Murray, "The crystal structures of $\text{Cu}_{1.8}\text{Se}$, Cu_3Se_2 , α - and γ - CuSe , CuSe_2 , and CuSe_2II ," *Canadian Journal of Chemistry*, vol. 54, no. 6, p. 841, 1976.
- [28] Z. Vucic, O. Milat, V. Horvatic, and Z. Ogorelec, "Composition-induced phase-transition splitting in cuprous selenide," *Physical Review B*, vol. 24, no. 9, pp. 5398–5402, 1981.
- [29] S. Kashida and J. Akai, "X-ray diffraction and electron microscopy studies of the room-temperature structure of Cu_2Se ," *J. Phys. C: Solid State Phys.*, vol. 5329–5336, no. 21, 1988.
- [30] A. Redinger, D. M. Berg, P. J. Dale, R. Djemour, G. Levent, T. Eisenbarth, N. Valle, and S. Siebentritt, "Route toward high-efficiency single-phase $\text{Cu}_2\text{ZnSn}(\text{S,Se})_4$ thin-film solar cells: model experiments and literature review," *IEEE Journal of Photovoltaics*, vol. 1, no. 2, pp. 200–206, 2011.
- [31] C. M. Fella, A. R. Uhl, Y. E. Romanyuk, and A. N. Tiwari, " $\text{Cu}_2\text{ZnSnSe}_4$ absorbers processed from solution deposited metal salt precursors under different selenization conditions," *Phys. Status Solidi (A)*, vol. 209, no. 6, pp. 1043–1048, Jun. 2012.
- [32] Z. Q. Li, J. H. Shi, Q. Q. Liu, Y. W. Chen, Z. Sun, Z. Yang, and S. M. Huang, "Large-scale growth of $\text{Cu}_2\text{ZnSnSe}_4$ and $\text{Cu}_2\text{ZnSnSe}_4/\text{Cu}_2\text{ZnSnS}_4$ core/shell nanowires," *Nanotechnology*, vol. 22, no. 26, p. 265615, Jul. 2011.

- [33] P. Uday Bhaskar, G. Suresh Babu, Y. B. Kishore Kumar, and V. Sundara Raja, "Investigations on co-evaporated Cu_2SnSe_3 and $\text{Cu}_2\text{SnSe}_3\text{-ZnSe}$ thin films," *Applied Surface Science*, vol. 257, no. 20, pp. 8529–8534, Aug. 2011.
- [34] A. J. Smith, P. E. Meek, and W. Y. Liang, "Raman scattering studies of SnS_2 and SnSe_2 ," *Journal of Physics and Chemistry of Solids*, vol. 10, 1977.
- [35] B. Minceva-Sukarova, M. Najdoskia, I. Grozdanova, and C. J. Chunnillalb, "Raman spectra of thin solid films of some metal sulfides," *Journal of Molecular Structure*, vol. 410–411, pp. 267–270, 1997.
- [36] B. B. Sharma, R. Ayyar, and H. Singh, "Stability of tetrahedral phase in the $\text{A}_2\text{B}^{\text{IV}}\text{C}_3^{\text{VI}}$ group of compounds," *Physica Status Solidi (a)*, vol. 40, no. 2, pp. 691–696, 1977.
- [37] J.-J. Wang, J.-S. Hu, Y.-G. Guo, and L.-J. Wan, "Wurtzite $\text{Cu}_2\text{ZnSnSe}_4$ nanocrystals for high-performance organic–inorganic hybrid photodetectors," *NPG Asia Materials*, vol. 4, no. 1, p. e2, Jan. 2012.

Appendix

COPYRIGHT PERMISSION DOCUMENTS



COPYRIGHT PERMISSION REQUEST

Please complete all contact information:

Name: Fei fei Feng Title: _____
Company/Organization: University of Delaware
Address: 7614 24th Ave.
City/State/Zip/Country: Hyattsville, MD, 20783
Phone: 302 766 3055 Email: feifeng@udel.edu

I am preparing an article/chapter for publication in the following formats (check as applicable):
Print Only ☐ Internet Only ☒ Print and Electronic Media ☐

The information will be used for (check as applicable):
Journal article ☐ Conference presentation ☐ Internal company records ☐
Dissertation ☒ Student course material ☐ Commercial publication* ☐

Please complete the following:

The article/chapter title will be: Cu₂ZnSnSe₄ Sonochemistry synthesis and Characterization.
The publication title will be: Master Thesis
Publisher: _____
Planned date of publication: _____

I hereby request permission for non-exclusive world rights for the above publication and all subsequent editions, revisions, and derivative works in English and foreign translations, in the formats indicated above from the following copyrighted content by ASM International:

Book ISBN: 978-0871704030 Copyright date: 1990
Book/Publication title: Binary Alloy Phase Diagram
Author name(s): T.B. Massalki, H. Okamoto
Article title: _____
Text page numbers: P 1476, P 3343, P 3358
Figure numbers (with page numbers): _____
Table numbers (with page numbers): _____

Signature: Fei fei Feng Date: 9/7/13

FOR ASM INTERNATIONAL USE ONLY:

I (we) grant permission requested above. Please ensure that ASM International receives proper credit as publisher by citing the above ASM publication as a reference and including the following: Reprinted with permission of ASM International. All rights reserved www.asminternational.org

ASM International Representative: [Signature] Date: 9-10-13

*For Commercial Publications, a copyright permission fee of \$50 per figure will be assessed.
Exceptions can be made for reuse of content by its original authors.

ASM International, Permissions, 9639 Kinsman Road, Materials Park, Ohio 44073-0002
permissions@asminternational.org Phone: 440-338-5151 x5465, Fax: 440-338-8542

SUBMIT

**ELSEVIER LICENSE
TERMS AND CONDITIONS**

Sep 18, 2013

This is a License Agreement between Feifei Feng ("You") and Elsevier ("Elsevier") provided by Copyright Clearance Center ("CCC"). The license consists of your order details, the terms and conditions provided by Elsevier, and the payment terms and conditions.

All payments must be made in full to CCC. For payment instructions, please see information listed at the bottom of this form.

Supplier	Elsevier Limited The Boulevard, Langford Lane Kidlington, Oxford, OX5 1GB, UK
Registered Company Number	1982084
Customer name	Feifei Feng
Customer address	7614 24th Ave HYATTSVILLE, MD 20783
License number	3231711477291
License date	Sep 18, 2013
Licensed content publisher	Elsevier
Licensed content publication	Thin Solid Films
Licensed content title	Predicted formation reactions for the solid-state syntheses of the semiconductor materials Cu_2SnX_3 and $\text{Cu}_2\text{ZnSnX}_4$ ($X = \text{S}, \text{Se}$) starting from binary chalcogenides
Licensed content author	F. Hergert, R. Hock
Licensed content date	31 May 2007
Licensed content volume number	515
Licensed content issue number	15
Number of pages	4
Start Page	5953
End Page	5956
Type of Use	reuse in a thesis/dissertation
Portion	figures/tables/illustrations
Number of figures/tables /illustrations	1

Format	both print and electronic
Are you the author of this Elsevier article?	No
Will you be translating?	No
Order reference number	
Title of your thesis/dissertation	Cu ₂ ZnSnSe ₄ SONOCHEMISTRY SYNTHESIS and CHARACTERIZATION
Expected completion date	Sep 2013
Estimated size (number of pages)	50
Elsevier VAT number	GB 494 6272 12
Permissions price	0.00 USD
VAT/Local Sales Tax	0.0 USD / 0.0 GBP
Total	0.00 USD
Terms and Conditions	

INTRODUCTION

1. The publisher for this copyrighted material is Elsevier. By clicking "accept" in connection with completing this licensing transaction, you agree that the following terms and conditions apply to this transaction (along with the Billing and Payment terms and conditions established by Copyright Clearance Center, Inc. ("CCC"), at the time that you opened your Rightslink account and that are available at any time at <http://myaccount.copyright.com>).

GENERAL TERMS

2. Elsevier hereby grants you permission to reproduce the aforementioned material subject to the terms and conditions indicated.

3. Acknowledgement: If any part of the material to be used (for example, figures) has appeared in our publication with credit or acknowledgement to another source, permission must also be sought from that source. If such permission is not obtained then that material may not be included in your publication/copies. Suitable acknowledgement to the source must be made, either as a footnote or in a reference list at the end of your publication, as follows:

"Reprinted from Publication title, Vol /edition number, Author(s), Title of article / title of chapter, Pages No., Copyright (Year), with permission from Elsevier [OR APPLICABLE SOCIETY COPYRIGHT OWNER]." Also Lancet special credit - "Reprinted from The Lancet, Vol. number, Author(s), Title of article, Pages No., Copyright (Year), with permission from Elsevier."

4. Reproduction of this material is confined to the purpose and/or media for which

permission is hereby given.

5. Altering/Modifying Material: Not Permitted. However figures and illustrations may be altered/adapted minimally to serve your work. Any other abbreviations, additions, deletions and/or any other alterations shall be made only with prior written authorization of Elsevier Ltd. (Please contact Elsevier at permissions@elsevier.com)

6. If the permission fee for the requested use of our material is waived in this instance, please be advised that your future requests for Elsevier materials may attract a fee.

7. Reservation of Rights: Publisher reserves all rights not specifically granted in the combination of (i) the license details provided by you and accepted in the course of this licensing transaction, (ii) these terms and conditions and (iii) CCC's Billing and Payment terms and conditions.

8. License Contingent Upon Payment: While you may exercise the rights licensed immediately upon issuance of the license at the end of the licensing process for the transaction, provided that you have disclosed complete and accurate details of your proposed use, no license is finally effective unless and until full payment is received from you (either by publisher or by CCC) as provided in CCC's Billing and Payment terms and conditions. If full payment is not received on a timely basis, then any license preliminarily granted shall be deemed automatically revoked and shall be void as if never granted. Further, in the event that you breach any of these terms and conditions or any of CCC's Billing and Payment terms and conditions, the license is automatically revoked and shall be void as if never granted. Use of materials as described in a revoked license, as well as any use of the materials beyond the scope of an unrevoked license, may constitute copyright infringement and publisher reserves the right to take any and all action to protect its copyright in the materials.

9. Warranties: Publisher makes no representations or warranties with respect to the licensed material.

10. Indemnity: You hereby indemnify and agree to hold harmless publisher and CCC, and their respective officers, directors, employees and agents, from and against any and all claims arising out of your use of the licensed material other than as specifically authorized pursuant to this license.

11. No Transfer of License: This license is personal to you and may not be sublicensed, assigned, or transferred by you to any other person without publisher's written permission.

12. No Amendment Except in Writing: This license may not be amended except in a writing signed by both parties (or, in the case of publisher, by CCC on publisher's behalf).

13. Objection to Contrary Terms: Publisher hereby objects to any terms contained in any purchase order, acknowledgment, check endorsement or other writing prepared by you, which terms are inconsistent with these terms and conditions or CCC's Billing and Payment terms and conditions. These terms and conditions, together with CCC's Billing and Payment

terms and conditions (which are incorporated herein), comprise the entire agreement between you and publisher (and CCC) concerning this licensing transaction. In the event of any conflict between your obligations established by these terms and conditions and those established by CCC's Billing and Payment terms and conditions, these terms and conditions shall control.

14. **Revocation:** Elsevier or Copyright Clearance Center may deny the permissions described in this License at their sole discretion, for any reason or no reason, with a full refund payable to you. Notice of such denial will be made using the contact information provided by you. Failure to receive such notice will not alter or invalidate the denial. In no event will Elsevier or Copyright Clearance Center be responsible or liable for any costs, expenses or damage incurred by you as a result of a denial of your permission request, other than a refund of the amount(s) paid by you to Elsevier and/or Copyright Clearance Center for denied permissions.

LIMITED LICENSE

The following terms and conditions apply only to specific license types:

15. **Translation:** This permission is granted for non-exclusive world **English** rights only unless your license was granted for translation rights. If you licensed translation rights you may only translate this content into the languages you requested. A professional translator must perform all translations and reproduce the content word for word preserving the integrity of the article. If this license is to re-use 1 or 2 figures then permission is granted for non-exclusive world rights in all languages.

16. **Website:** The following terms and conditions apply to electronic reserve and author websites:

Electronic reserve: If licensed material is to be posted to website, the web site is to be password-protected and made available only to bona fide students registered on a relevant course if:

This license was made in connection with a course,

This permission is granted for 1 year only. You may obtain a license for future website posting,

All content posted to the web site must maintain the copyright information line on the bottom of each image,

A hyper-text must be included to the Homepage of the journal from which you are licensing at <http://www.sciencedirect.com/science/journal/xxxxx> or the Elsevier homepage for books at <http://www.elsevier.com>, and

Central Storage: This license does not include permission for a scanned version of the material to be stored in a central repository such as that provided by Heron/XanEdu.

17. **Author website** for journals with the following additional clauses:

All content posted to the web site must maintain the copyright information line on the bottom of each image, and the permission granted is limited to the personal version of your

paper. You are not allowed to download and post the published electronic version of your article (whether PDF or HTML, proof or final version), nor may you scan the printed edition to create an electronic version. A hyper-text must be included to the Homepage of the journal from which you are licensing at <http://www.sciencedirect.com/science/journal/xxxxx>. As part of our normal production process, you will receive an e-mail notice when your article appears on Elsevier's online service ScienceDirect (www.sciencedirect.com). That e-mail will include the article's Digital Object Identifier (DOI). This number provides the electronic link to the published article and should be included in the posting of your personal version. We ask that you wait until you receive this e-mail and have the DOI to do any posting.

Central Storage: This license does not include permission for a scanned version of the material to be stored in a central repository such as that provided by Heron/XanEdu.

18. **Author website** for books with the following additional clauses:

Authors are permitted to place a brief summary of their work online only.

A hyper-text must be included to the Elsevier homepage at <http://www.elsevier.com>. All content posted to the web site must maintain the copyright information line on the bottom of each image. You are not allowed to download and post the published electronic version of your chapter, nor may you scan the printed edition to create an electronic version.

Central Storage: This license does not include permission for a scanned version of the material to be stored in a central repository such as that provided by Heron/XanEdu.

19. **Website** (regular and for author): A hyper-text must be included to the Homepage of the journal from which you are licensing at <http://www.sciencedirect.com/science/journal/xxxxx>, or for books to the Elsevier homepage at <http://www.elsevier.com>

20. **Thesis/Dissertation**: If your license is for use in a thesis/dissertation your thesis may be submitted to your institution in either print or electronic form. Should your thesis be published commercially, please reapply for permission. These requirements include permission for the Library and Archives of Canada to supply single copies, on demand, of the complete thesis and include permission for UMI to supply single copies, on demand, of the complete thesis. Should your thesis be published commercially, please reapply for permission.

21. **Other Conditions**:

v1.6

If you would like to pay for this license now, please remit this license along with your payment made payable to "COPYRIGHT CLEARANCE CENTER" otherwise you will be invoiced within 48 hours of the license date. Payment should be in the form of a check or money order referencing your account number and this invoice number RLNK501115251.

**Once you receive your invoice for this order, you may pay your invoice by credit card.
Please follow instructions provided at that time.**

Make Payment To:
Copyright Clearance Center
Dept 001
P.O. Box 843006
Boston, MA 02284-3006

**For suggestions or comments regarding this order, contact RightsLink Customer
Support: customercare@copyright.com or +1-877-622-5543 (toll free in the US) or
+1-978-646-2777.**

**Gratis licenses (referencing \$0 in the Total field) are free. Please retain this printable
license for your reference. No payment is required.**
